Smart Structures and Systems, *Vol. 34, No. 3 (2024) 181-201*
https://doi.org/10.12989/sss.2024.34.3.181

Compressive strength of masonry structures through metaheuristics optimization algorithms

Ziqi Liu [1a], Hossein Moayedi*[2,3], Mehmet Akif Cifci [4,5b], Mohammad Hannan [6c] and Erkut Sayin [7d]

[1] *Department of Mechanical, Aerospace, and Civil Engineering, University of Manchester, UK*
[2] *Institute of Research and Development, Duy Tan University, Da Nang, Vietnam*
[3] *School of Engineering & Technology, Duy Tan University, Da Nang, Vietnam*
[4] *Department of Computer Engineering, Bandirma Onyedi Eylul University, 10200 Balikesir, Türkiye*
[5] *Engineering and Informatics Department, Klaipėdos Valstybinė Kolegija/Higher Education Institution, 92294 Klaipeda, Lithuania*
[6] *Department of Mathematics, Shiraz University of Technology, Shiraz, Iran*
[7] *Fırat University, Department of Civil Engineering, 23200 Elazığ, Türkiye*

(*Received October 7, 2023, Revised October 7, 2024, Accepted October 12, 2024*)

Abstract. This study presents a comparative analysis of three nature-inspired algorithms—Black Hole Algorithm (BHA), Earthworm Optimization Algorithm (EWA), and Future Search Algorithm (FSA)—for predicting the compressive strength of masonry structures. Each algorithm was integrated with a Multilayer Perceptron (MLP) model, using a structural dimension, rebound number, ultrasonic pulse velocity, and failure load dataset. The dataset was divided into training (70%) and testing (30%) subsets to evaluate model performance. Root Mean Square Error (RMSE) and the coefficient of determination (R^2) were employed as statistical indices to measure accuracy. The BHA-MLP model achieved the best performance, with an RMSE of 0.04731 and an R^2 of 0.9995 for the training dataset and an RMSE of 0.06537 and an R^2 of 0.99877 for the testing dataset, securing the highest overall score. FSA-MLP ranked second, demonstrating strong predictive performance, followed by EWA-MLP, which performed with lower accuracy but still showed valuable results. The study highlights the potential of using these nature-inspired optimization algorithms to enhance the predictive accuracy of compressive strength in masonry structures, offering insights for engineering and policymaking to improve structural safety and performance.

Keywords: compressive strength; masonry structures; metaheuristics; optimization

1. Introduction

Nondestructive Testing (NDT) methods are precious for determining the mechanical properties of masonry materials without causing damage to the structure. These techniques allow engineers and researchers to assess the quality, strength, and integrity of masonry materials such as bricks, stones, and mortar without removing or destroying any parts of the building or even structural dynamic response reconstruction (Shu *et al*. 2025). The structure's present damage state must be understood to estimate the remaining service life (Asteris *et al*. 2020, Koopialipoor *et al*. 2022, Zhao *et al*. 2024). Various standards offer various methods for keeping tabs on the condition of ancient buildings. Most recommendations, however, advocate a minimal intervention strategy that maintains structural integrity. The ICOMOS (Charter 2003) standards usually forbid doing irreversible harmful testing on antique structures that have historical significance. Core extraction is not recommended for historic sites with artwork, paintings, or graffiti on their walls since it might harm them (Faghfouri *et al*. 2023). Many masonry structures, mainly historical or heritage buildings or flexible bridges, cannot be subjected to destructive testing (Sun *et al*. 2025). NDT methods allow for assessing mechanical properties without compromising the structure's integrity. Integrating NDT data with several testing methods for older buildings is advised to identify the parameter of interest. The data from nondestructive testing must be transformed to provide relevant damage indicators. Furthermore, taking core samples from the structure may give inaccurate findings if the samples are not representative. Techniques for NDT help determine the masonry material's mechanical properties and the overall level of damage. Utilizing NDT methods to evaluate structural damage helps save costs, time, and aesthetics.

The compressive strength of masonry is crucial for understanding its ability to support loads. It is the most used condition indicator for determining the state of masonry constructions' deterioration. The compressive strength of a structure is affected by its age, the durability of its constituent parts (brick and mortar units), the thickness of the mortar joints, and the level of craftsmanship used (Köksal *et al*. 2005). The right choices may be made to repair, refit, and rehabilitate a building to extend its service

*Corresponding author, Ph.D.,
E-mail: hosseinmoayedi@duytan.edu.vn
[a] M.Sc., E-mail: liuziqi-liu@outlook.com
[b] Ph.D., E-mail: mcifci@bandirma.edu.tr
[c] Former Student M.Sc.,
E-mail: mohammad.hannan.MH@gmail.com
[d] Ph.D., E-mail: esayin@firat.edu.tr

ISSN: 1738-1584 (Print), 1738-1991 (Online)

life if the damaged sites are understood. NDT methods can estimate this property by analyzing surface hardness or material density.

Brick or stone masonry of various sizes was formerly used to build masonry constructions. Masonry constructions may range in size from modest huts to substantial structures like forts and castles (Yoon and Lee 2023). Chen *et al*. (2024) focus on enhancing the ultimate bearing capacity of these composite structures, which combine steel's strength with concrete's ductility. Through experimental testing, the study evaluates how the reinforced concrete filling improves load-bearing capacity, delays buckling, and increases overall flexibility and stability. The results highlight the effectiveness of high-ductility concrete in reinforcing thin-walled steel tubes, making them suitable for applications requiring high strength and flexibility, such as in seismic-prone regions. Removing core samples is costly in determining the compressive strength of historic structures that have already sustained damage. According to Masi and Chiauzzi (2013), NDT might drastically decrease the total number of concrete cores that need to be removed, lowering costs and maintaining the structural integrity of the reinforced concrete structure. Indirect test results from NDT are employed to calculate compressive strength. The rebound hammer test measures a material's hardness (rebound hammer value RH) and is non-destructive. Brick masonry's compressive strength (f_c) and hardness are connected (Brencich and Sterpi 2006). Since the rebound hammer test does not directly provide the compressive strength value, it is an indirect test. Ultrasonic pulse velocity (UPV) for precisely determining concrete compressive strength and elastic modulus in concrete specimens has become more common (Bogas *et al*. 2013, Sabbağ and Uyanık 2017, Zhou *et al*. 2020).

In modern construction, it is essential to consider the technical aspects of structural performance and the broader socioeconomic and environmental impacts (Ali *et al*. 2024), optimization of multi-material active structures to reduce energy consumption and carbon footprint (Kardani *et al*. 2022, Wang and Sigmund 2023, 2024), or understanding and evaluating the structural behavior and mechanical performance of Glulam (glued laminated timber) connections that use slotted-in steel plates and multiple bolts. (Cao *et al*. 2024)

Smart structures are increasingly recognized for their potential to optimize resource efficiency and minimize environmental footprints. Socioeconomic indicators, such as construction costs, labor efficiency, and long-term maintenance, are critical in determining the feasibility of adopting advanced materials and techniques in the industry. For instance, in-wall design, special attention must be given to areas (also called thermal bridges) where heat transfer is likely to increase (e.g., around windows, doors, or joints). These areas can lead to higher heat loss without proper insulation or design. Some scholars used numerical simulation to find relations between heat transfer (a critical factor in concrete masonry wall design, influencing decisions about wall materials, thickness, and insulation) (Haddadvand *et al*. 2024, Sohrabi *et al*. 2024).

Integrating metaheuristic optimization algorithms into the design and management of intelligent structures can drive cost reductions by improving material utilization and enhancing the longevity of structures, thereby reducing the need for frequent repairs or replacements. Environmental indicators, such as carbon emissions, energy consumption, and the use of sustainable materials, are also central to the study. As construction activities are among the most significant contributors to global carbon emissions, optimizing compressive strength through advanced computational techniques can develop more durable and resilient structures, thus reducing material waste and energy consumption. Including such indicators in this study underscores the growing need for sustainable construction practices, aligning with global objectives for reducing environmental impact and promoting socioeconomic growth through more intelligent, more efficient building systems (Poorisat *et al*. 2024).

Armaghani *et al*. (2021) investigated using two nondestructive testing methods to estimate granite's unconfined compressive strength (UCS). By focusing on the Schmidt hammer rebound value and the ultrasonic pulse velocity, the study demonstrates that these two easily measurable parameters can provide accurate predictions of granite's UCS. The research highlights the efficiency of using minimal nondestructive test data to estimate rock strength, offering a practical and cost-effective approach for geotechnical applications and minimizing the need for extensive destructive testing. In addition, Alkayem *et al*. (2023) provide a comprehensive review of the latest advancements in the use of machine learning (ML) and deep learning (DL) for predicting the behavior of concrete and FRC when exposed to high temperatures. The review highlights how these techniques improve the accuracy of predicting crucial properties such as compressive strength, thermal resistance, and durability under extreme conditions. The paper discusses the benefits of ML/DL models over traditional methods, addressing their ability to handle large datasets and complex material behaviors. It also outlines current challenges and potential future directions, emphasizing the need for more data and improved model generalization to enhance predictions in real-world applications.

Lu *et al*. (2017) proposed a mathematical model to describe how concrete behaves under dynamic (rapidly applied) uniaxial loads, such as those experienced during impacts, explosions, or earthquakes. This criterion accounts for the fact that concrete's strength can increase under dynamic loading conditions compared to static loading.

Using Artificial Neural Networks (ANN) for estimating the compressive strength of masonry buildings is a practical approach due to ANN's ability to model complex, non-linear relationships between input variables and target outputs (Wang *et al*. 2024, Wu *et al*. 2024, Ye *et al*. 2024). A shorter learning curve, more accessible analysis, better prediction accuracy, and flexibility in response to the compressive strength of masonry buildings are further benefits of ANN methods over other approaches, such as statistical techniques and simulation. This work provides an example of using the ANN approach to compressive strength of masonry buildings. The input layer of an ANN's

computational architecture accepts environmental patterns as input, while the output layer shows a reaction to environmental circumstances (Ahmadi Dehrashid *et al*. 2024, Moayedi *et al*. 2024, Moayedi and Le 2024b). More layers link input and output while staying covert and avoiding direct contact with the outer world. Input weights, biases, and transfer functions make up these parameters. To train a neural network, adjust the weights until the expected and actual outputs are almost identical. The interactions between the input, hidden, and output layers shape a neural network model. Feedforward, competitive, recurrent associative memory and semantic segmentation networks are among the several types of networks most often employed in ANN applications (Moayedi *et al*. 2022, Moayedi and Khasmakhi 2022, Wang and Sigmund 2023, Chai *et al*. 2024). A specific set of learning principles could apply to each kind of network. Reinforcement (or graded) learning rules, unsupervised learning rules, and supervised learning rules are the three broad categories of learning rules. Readers with various levels of technical expertise may comprehend the neural network theory described by Zurada (1992) since it has been studied extensively along with the development of the technique. ANN approaches are explained in detail and illustrated with examples from real-world applications in Hagan *et al*. (1997) work.

Christopher *et al*. (2023) studied self-compacting polyester fiber-reinforced concrete and strength prediction by ANN. Asteris *et al*. (2024) developed ANN models to predict rocks' uniaxial compressive strength (UCS) by incorporating key parameters such as porosity, compressional wave velocity, and Schmidt hammer rebound values. These parameters were chosen due to their strong correlation with rocks' mechanical properties and relative ease of measurement in field and laboratory conditions. The ANN models were trained using a dataset of rock samples, and their predictive performance was evaluated against actual UCS values. The results showed that the ANN models provided high accuracy in predicting UCS, outperforming traditional regression methods. Integrating multiple input variables in the ANN models enhanced their predictive capability, making them a powerful tool for estimating rock strength in geotechnical and mining engineering applications. Asteris *et al*. (2021) explore the application of various machine-learning algorithms to predict the compressive strength of cement-based mortars. By utilizing input parameters such as the composition of the mortar mix, curing time, and environmental factors, the study demonstrates how machine learning models, including decision trees, support vector machines, and artificial neural networks, can accurately estimate compressive strength. The findings highlight that machine learning techniques outperform traditional predictive methods, offering a more reliable and efficient approach for optimizing construction and material science mortar formulations.

The compressive strength of masonry and smart structures ensures structural integrity, durability, and safety in modern construction. While traditional methods of assessing and optimizing compressive strength have provided valuable insights, they often fail to account for the complexity and variability inherent in smart materials and systems. Metaheuristic optimization algorithms offer a promising alternative by enhancing prediction accuracy and optimization capability, particularly when combined with machine learning models like MLP. This research addresses the growing demand for advanced computational methods to optimize smart structures' performance in response to various environmental and load-bearing conditions. Second, the study contributes to the limited knowledge of applying metaheuristic algorithms—such as FSA, BHA, and EWA—to structural optimization. By demonstrating that BHA-MLP offers superior accuracy (R^2 = 0.9995), this research highlights the potential of these methods for improving predictive performance over conventional techniques. In recent years, numerous studies have explored machine learning and metaheuristic optimization techniques for predicting the compressive strength of various structures, including masonry and intelligent structures. These studies aim to improve the accuracy of predictions compared to traditional statistical and empirical models (Table 1).

Moreover, the novelty of this work lies in the systematic comparison of these three metaheuristic algorithms,

Table 1 A brief overview of relevant research and their error results

Ref.	Case study	Methods of study	R^2 results
(Mishra *et al*. 2020a)	compressive strength of unreinforced brick masonry	SVR ANN ANFIS	0.962 0.963 0.985
(Ronghui and Liangrong 2022)	optimization of building material in construction management	PSO-train PSO-test	0.9899 0.9867
(Algaifi *et al*. 2021)	compressive strength of smart bio-concrete	ANN ANFIS	0.985 0.986
(Marani and Nehdi 2020)	compressive strength for phase change materials integrated cementitious composites	RFR ETR GBR XGBR	0.939 9.957 0.977 0.969
(Alyami *et al*. 2024)	compressive strength of 3D printed fiber-reinforced concrete	DT RF GB GEP	0.987 0.986 0.986 0.98

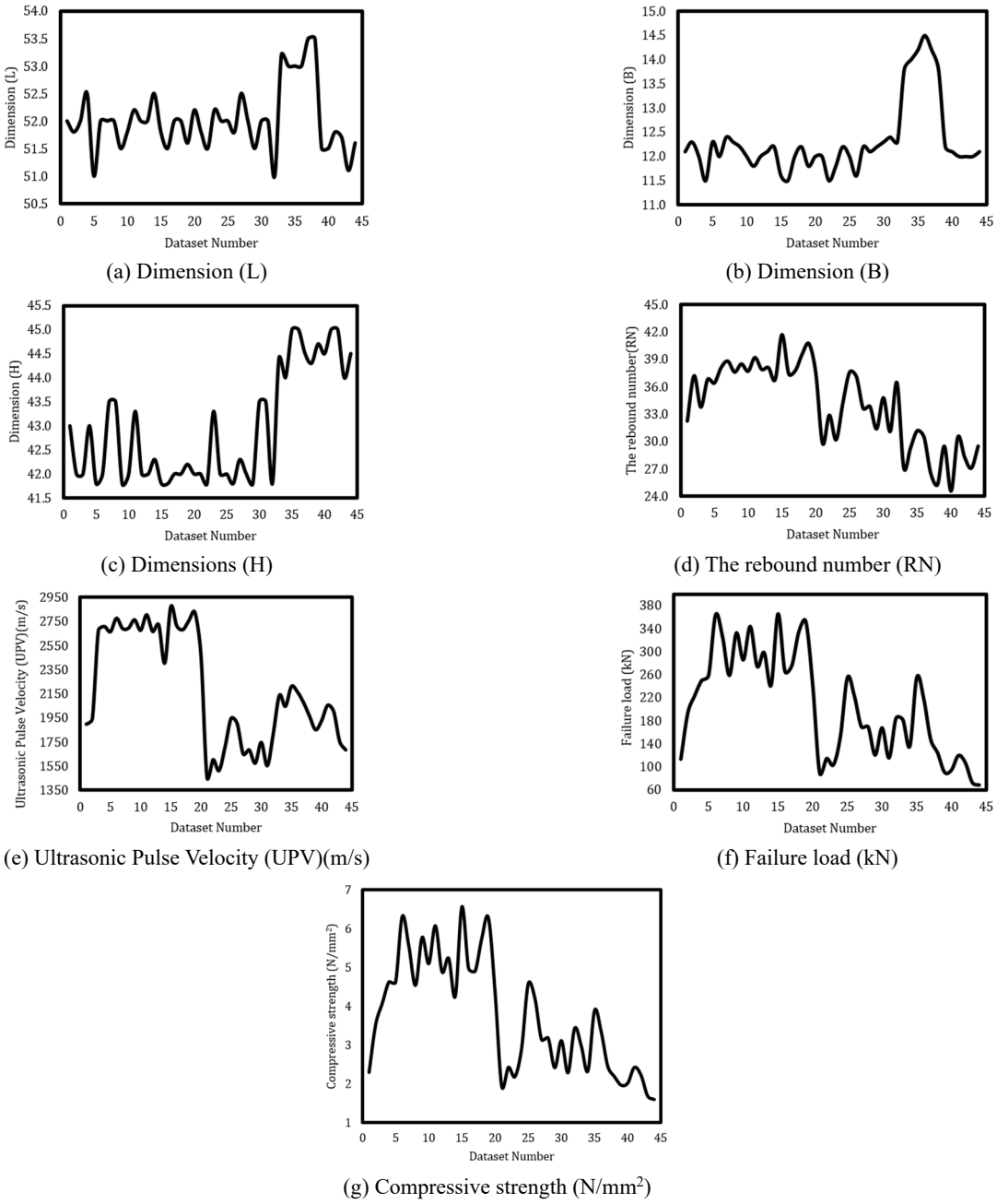

Fig. 1 Variation of input and output parameters; input parameter: (a) Dimension (L); (b) Dimension (B); (c) Dimension (H); (d) The rebound number (RN); (e) Ultrasonic Pulse Velocity (UPV)(m/s); (f) Failure load (kN); output parameter: (g) Compressive strength (N/mm^2)

providing engineers and researchers with evidence-based insights into the most effective tools for compressive strength optimization. As smart structures evolve, this research paves the way for more adaptive, intelligent design processes, fostering safety and innovation in the construction industry.

2. Established database

Mishra *et al*. (2021) indicated that direct compressive strength tests are used in a thorough laboratory inquiry to assess the compressive strength of brick, mortar, and brick-mortar masonry wallets. Before evaluating the combined units, NDT was carried out on masonry wallets and separate brick-and-mortar units. Three stages of tests for bricks, mortar, and wallets are used to study masonry and mortar units (Mishra *et al*. 2021). The dataset parameters were carefully chosen for their direct impact on the compressive strength of masonry structures. The combination of geometric dimensions, nondestructive test results, and failure load provides a comprehensive set of inputs for predicting compressive strength with metaheuristic optimization algorithms. This selection enhances the accuracy of the models and enables compelling predictions, which can lead to more efficient and safer structural designs

in smart systems. Fig. 1 illustrates inputs and output parameters.

The input parameters used in the models and the rationale behind their selection are illustrated below:

Dimension (*L*) - Length (mm): The masonry structure or component length. This parameter is crucial in the material's structural load distribution and stress behavior. Length affects the structural stability and load-bearing capacity of masonry units. Variations in length can influence the overall compressive strength as more extended elements may behave differently under load due to potential buckling or stress concentration points.

Dimension (*B*) - Breadth (mm): The breadth or width (or thickness) of the masonry structure or unit. Like the length, the breadth influences the load distribution across the structure. Breadth, in combination with length, contributes to the cross-sectional area of the masonry element, which is directly linked to the load-bearing capacity. A wider breadth increases the area that resists compressive loads, potentially leading to higher compressive strength.

Dimension (*H*) - Height (mm): The height of the masonry structure or component. Height impacts the slenderness ratio of the structure, which is a critical factor in determining its susceptibility to buckling or failure under compression. Taller structures may have different stress distributions than shorter ones, making height a significant parameter in the compressive strength prediction model.

Rebound Number (*RN*): The rebound number is obtained from the Schmidt hammer test, a nondestructive test method for evaluating the surface hardness of materials. The rebound number directly correlates with the surface strength of masonry structures. Higher rebound numbers indicate more complex, durable surfaces, often linked to higher compressive strength. The RN is commonly used in structural assessments due to its simplicity and ability to provide rapid surface strength estimations.

Ultrasonic Pulse Velocity (*UPV*) **(m/s):** The UPV measures the velocity of an ultrasonic pulse through the material, indicating its density and internal integrity. The UPV is a crucial parameter for evaluating the quality and uniformity of masonry materials. A higher UPV usually reflects better material quality, with fewer internal voids or cracks, which correlates with higher compressive strength. This parameter is handy in nondestructive testing to identify defects that might not be visible on the surface but could reduce the overall structural strength.

Failure Load (*kN*): The failure load is the maximum load that the masonry structure can withstand before failure (collapse or fracture) occurs. The failure load directly reflects the structure's load-bearing capacity under real-world conditions. It is a primary indicator of the material's strength under compression. The failure load is essential for predicting the compressive strength as it directly represents the ultimate capacity of the material under stress.

Compressive Strength (N/mm²) as the main Output Parameter: Compressive strength represents the maximum compressive stress the material can withstand before failure. It is measured in Newton per square millimeter (N/mm²). Compressive strength is the most critical parameter in assessing the performance of masonry and intelligent structures, especially in load-bearing applications. It directly impacts the material's structural safety, durability, and longevity. The goal of the model is to predict this value based on the input parameters, providing insights into how various physical properties and nondestructive test results correlate with the material's overall strength.

Each parameter chosen directly or indirectly impacts the compressive strength of masonry structures. For example, geometric dimensions (length, breadth, height) influence structural stability and load distribution. At the same time, the rebound number and UPV offer insights into the material's surface hardness and internal consistency, which are critical for understanding its compressive behavior. Parameters like the rebound number and UPV are derived from widely accepted nondestructive testing methods. These parameters are popular in structural assessment because they allow engineers to evaluate the material's properties without damaging the structure. This is particularly useful in smart structures, where continuous monitoring is needed to maintain performance. The failure load directly measures the structure's performance under compression, providing a real-world benchmark for the compressive strength models. The models aim to predict compressive strength with higher accuracy by correlating the failure load with other parameters. The parameters were selected based on their relevance to structural behavior in classical and intelligent materials. Engineers and researchers have long used these measurements to evaluate masonry strength and quality. These parameters were chosen due to their accessibility and the practicality of obtaining them in real-world testing environments. Nondestructive testing methods like UPV and Schmidt hammer (rebound number) are common in structural engineering, making these parameters practical for large-scale testing and data collection. The parameters were tested for their statistical significance in predicting compressive strength. By analyzing the correlation between the input variables and the output (compressive strength), the researchers ensured that the selected parameters contributed meaningful information to the predictive models.

To ensure the replicability of this study, a detailed explanation of the data preprocessing steps is crucial. The raw dataset used in this research, consisting of parameters such as Dimension (L, B, H), Rebound Number (RN), Ultrasonic Pulse Velocity (UPV), and Failure Load, was preprocessed through the following stages:

- ***Data Cleaning*:** The dataset was first inspected for missing or erroneous values. Missing values, if any, were handled using interpolation methods, and any outliers detected during this inspection were analyzed to determine their relevance or were removed if proven to be erroneous.
- ***Normalization*:** Since the dataset contained parameters with different units and scales (e.g., dimensions in millimeters, UPV in meters per second), normalization was applied to ensure uniformity. Min-max normalization was used to scale the values of all input parameters between 0

Table 2 Mean, minimum, maximum, and std values of data parameters

	Dimension (L)	Dimension (B)	Dimension (H)	Rebound number (RN)	Ultrasonic Pulse Velocity (UPV) (m/s)	Failure Load (kN)	Compressive Strength (N/mm²)
Mean	52.0	12.3	42.9	34.0	2191	206.17	3.24045
Min	51.0	11.5	41.8	24.6	1458	68.050	1.090
Max	53.5	14.5	45.0	41.7	2870	365.27	6.070
Std. Deviation	0.58	0.75	1.16	4.51	460.7	89.0	1.46

and 1, which prevents any one parameter from disproportionately influencing the model's training process.

- ***Feature Selection*:** All input parameters were retained as each had a significant contribution to the prediction of compressive strength. No additional feature selection methods were applied as the parameters were predetermined based on domain expertise and prior studies.
- ***Data Splitting*:** The dataset was randomly split into training (70%) and testing (30%) sets to evaluate the models' performance unbiasedly. The split maintained the integrity of the data distribution to ensure that the training set represented a broad range of scenarios for model learning, and the testing s*et al*lowed for a fair assessment of predictive performance.
- ***Data Augmentation*** (if applicable): In cases where the dataset was limited, synthetic data generation techniques such as SMOTE (Synthetic Minority Over-sampling Technique) were considered to ensure that the model had sufficient data for training, particularly for scenarios with underrepresented structural configurations.

Following the above data preprocessing steps, the models were trained and tested on a normalized, well-distributed dataset, ensuring high accuracy and reliability in predicting compressive strength. These steps are fundamental for replicating the results and can serve as a guideline for future research using similar datasets and methodologies.

3. Methodology

The approach included several crucial elements to guarantee the accuracy of the susceptibility prediction. Fig. 2 depicts the methodology's process from data collection through susceptibility prediction. The preparation and collection of relevant data required for modeling the compressive strength of masonry structures; the collection of data from field experiments observed regarding this strength; the modeling of this strength using the BHA-MLP, EWA-MLP, and FSA-MLP models; and the performance assessment of the models.

In selecting the nature-inspired algorithms—Black Hole Algorithm (BHA), Earthworm Optimization Algorithm (EWA), and Future Search Algorithm (FSA)—this study aimed to leverage their unique strengths in solving complex optimization problems. These algorithms were chosen over others based on their distinctive features and proven effectiveness in handling non-linear, multi-dimensional optimization tasks, which are crucial for predicting compressive strength in masonry structures.

The BHA was chosen for its simplicity and efficiency in converging to optimal solutions. Inspired by the concept of black holes in space, this algorithm mimics the gravitational pull that attracts neighboring stars. The advantage of BHA lies in its ability to exploit a solution space effectively while avoiding local optima—a critical feature for predicting compressive strength where the search space is vast and complex. Additionally, BHA has a robust exploration mechanism ensures a comprehensive solution space search, making it ideal for highly dynamic and uncertain environments such as intelligent structures. The black hole represents the best solution, and as the algorithm iterates, it pulls other candidate solutions (stars) toward it. Poor-performing solutions are eliminated, mimicking how stars crossing the event horizon are absorbed by the black hole, allowing the algorithm to focus on the most promising areas of the solution space.

The EWA was selected for its robust local search capability, inspired by the natural behavior of earthworms moving through the soil. This algorithm is particularly effective in fine-tuning solutions in the later stages of optimization, making it suitable for compressive strength prediction, where precision is paramount. EWA balances exploration and exploitation by modeling earthworms' behaviors of spreading and shrinking during their movement. This characteristic allows the algorithm to maintain diversity in the population of solutions while converging to high-quality solutions. In EWA, candidate solutions (earthworms) spread across the search space, with each iteration adjusting their positions based on both global and local search strategies. This mimics how earthworms efficiently explore the soil to find nutrients, which, in optimization terms, translates to the algorithm's ability to analyze the solution space effectively and refine the best solutions.

FSA was chosen for its advanced search strategy, which integrates foresight and adaptability in locating optimal solutions. This algorithm simulates a decision-making process that explores future potential outcomes based on current data. It is particularly suitable for dynamic systems like innovative structures, where conditions and factors influencing compressive strength may change over time. The FSA excels in multi-objective optimization problems, where multiple conflicting criteria must be balanced, such as maximizing strength while minimizing material use. FSA operates by generating a variety of potential future states (candidate solutions) and evaluating them based on predicted outcomes. It then refines the current solution by selecting future states with the most promise. It effectively searches the solution space with a long-term perspective,

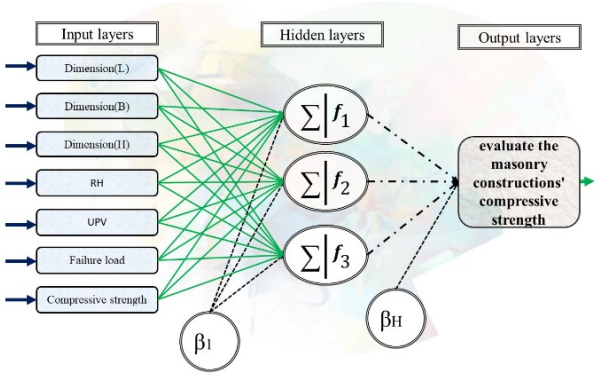

Fig. 2 An illustration of the suggested MLP approach

which helps avoid premature convergence and improves the overall solution quality.

These algorithms were selected because they balance exploration (searching broadly across the solution space) and exploitation (refining the best solutions). For compressive strength prediction, this balance is essential, as it allows the models to capture complex relationships between input parameters while fine-tuning predictions for better accuracy. The BHA, EWA, and FSA are scalable and flexible, which means they can handle the multi-dimensionality of the dataset (e.g., physical dimensions, material properties) without significant computational overhead. Their ability to adapt to varying problem sizes and types ensures they can effectively apply to diverse structural configurations and conditions. These algorithms have been successfully used in various engineering and optimization fields, showing superior performance in finding optimal solutions to complex, multi-modal problems. Their inclusion in this study ensures that predictions are robust, accurate, and generalizable across different scenarios.

By choosing BHA, EWA, and FSA, this study capitalizes on their distinct strengths in handling complex optimization tasks, making them well-suited for accurately predicting the compressive strength of masonry structures in intelligent systems. The unique features of these algorithms—BHA's intense global search, EWA's efficient local refinement, and FSA's future-oriented approach—provide a comprehensive solution to the challenges posed by this study's optimization problem.

3.1 Artificial neural network

The artificial neural network makes it easier to model complicated systems in approximation issues, such as finance, engineering (Mishra *et al*. 2020b), and medicine. As a system for processing and analyzing data, an artificial neural network mimics the structure and operations of the human brain. ANNs may be thought of as densely networked, multilayered structures made up of many neurons. When additional input words are given after correctly predicting the recommended output pattern, such a network can spot similarities. Artificial neural networks may replace several intricate statistical analysis techniques, including autocorrelation, linear regression, trigonometric analysis, and multivariable regression (Bilgehan and Turgut 2010). The three essential elements stated below—transfer function, network design, and learning law—can be used to define ANN, an established network (Kubat 1995). After considering these variables, the best model is chosen for a particular problem or set of issues. For neural networks, several different training techniques have been developed. The most accurate and reliable algorithms out of these are feedforward neural networks (FFNNs) and the back-propagation (BP) method. For instance, back-propagation is one of the most well-liked artificial neural network training algorithms because it can solve geotechnical problems that are predictably difficult. One of the most popular types of neural networks, feedforward neural networks, can have several hidden layers containing bias vectors, nonlinear transfer functions, and weight matrices. This network could be trained to find complex nonlinear correlations between input and output datasets.

Given that neural network-generated relations are not precise, one may always expect a discrepancy between the actual data and the networks' estimated data due to the extracted relations' imprecision. It is required to calibrate the bias and weight components, which are constants that may be changed, to reduce network error. Network training is the process of learning these constants. Similar to how an optimization process works, training does, too. Many fundamentally analytical mathematical methods, including Bayesian regularization (BR), BFGS quasi-Newton (BFG), and Levenberg Marquardt (LM), are utilized to train neural networks. In the current investigation, networks were trained in batches using the Levenberg-Marquardt method.

As suggested by Liou *et al*. (2009), to facilitate the design process during the initial phase of modeling an ANN, the following equation is used to normalize the developed datasets

$$X_{norm} = (X - X_{min})/(X_{max} - X_{min}) \quad (1)$$

In which X_{norm} and X are the normalized and measured values, respectively. X_{min} and X_{max} are the minimum and maximum X values.

Subsequently, to develop and evaluate the model, the whole dataset should be divided into training and testing sets, respectively. In their investigation, McCord-Nelson and Illingworth (1991) have recommended using a range of 20–30% of all datasets for testing datasets. As a result, the present study allocated 20% of all datasets to the testing datasets. Many studies have referred to the successful use of the Levenberg Marquardt training algorithm. As a result, the present paper used the same algorithm to design the artificial neural network. In addition, it has been shown that artificial neural networks featuring one hidden layer can approximate all continuous functions. To determine the number of hidden nodes, (Hornik *et al*. 1989) reported that the maximum number of hidden nodes is $\leq 2 \times \text{Ni} + 1$, in which Ni stands for the number of input layers. According to the same equation, a range of 1–10 seems to be solvable for the bearing capacity problem (Huang *et al*. 2021). After analyzing a series of artificial neural network models, the results were analyzed using the values of RMSE. The RMSE was the performance index most commonly used to

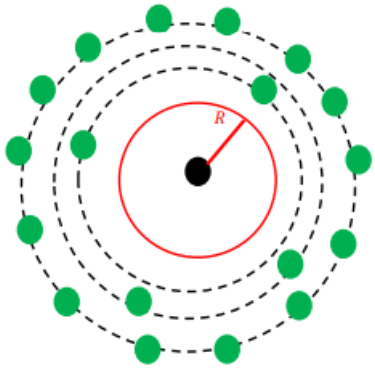

Fig. 3 Black Hole schema (Kumar *et al*. 2015)

evaluate the predictive models. The iterations characterized by five hidden nodes were the best among the whole-generated models. As a result, the 6 × 5 × 1 architecture was chosen as the optimal architecture of artificial neural networks to predict the specified network target.

3.2 Black Hole Algorithm (*BHA*)

A resilient stochastic optimization method called the black hole optimization algorithm is based on describing how a black hole behaves in space (Kumar *et al*. 2015). The procedures listed below describe how to simulate the BHA from the black hole phenomenon:

Step 1: There are both known and undiscovered stars in the universe. Since individual stars collide to generate black holes, BHA starts with a population of stars randomly distributed throughout the universe. Each star in BHA has a fitness value assessed and optimized using a fitness function. The black hole is chosen as the best star with the highest fitness value. BHA schema is shown in Fig. 3. Green circles are stars, while the black circle is a black hole. In the search area, they were scattered. It is dubbed "black" because it completely absorbs light and does not reflect any of it.

Step 2: A black hole is an object with a very high density and a powerful gravitational pull in the actual world. This results in a strong gravitational attraction on the stars nearby. BHA has acted in the same way. By Eq. (2), every star started to move in the direction of the black hole.

Step 3: The event horizon is the sphere-shaped boundary of a black hole in space. The Schwarzschild radius is the name given to the event horizon. The event horizon of a black hole is depicted by the red circle in Fig. 3. The Schwarzschild radius is calculated using Eq. (3) for real space and Eq. (4) for BHA.

Step 4: When a star crosses the event horizon of a black hole, it will be absorbed by it and vanish due to the black hole's high gravity and density. Nothing can escape from within the event horizon since the escapee's speed is equivalent to the speed of light there. BHA calculates the Euclidean distance between a black hole and a star. Replace it with a new star in a random position in the search space if the distance is less than the Schwarzschild radius.

Step 5: In BHA, if a star travels to a less expensive location than a black hole, its position should be changed.

$$X_i(t+1) = X_i(t) + rand \times \left(X_{BH} - X_i(t)\right) \quad i = 1, 2, \ldots, N \tag{2}$$

$$R = 2GM/C^2 \tag{3}$$

$$R = \frac{f_{BH}}{\sum_{i=1}^{N} f_i} \tag{4}$$

where $X_i(t)$ and $X_i(t+1)$ denote the *i*th star's coordinates at iterations t and $t + 1$. Rand denotes a uniform distribution with a 0 to 1 scale. *N* stands for the number of stars. The symbol indicates the black hole's position in the exploration space. X_{BH}. The letters *M*, *G*, and *C* represent the gravitational constant, the black hole's mass, and the speed of light, respectively. The fitness value of the *i*th star is denoted by f_i, while the black hole's fitness value is denoted by f_{BH}.

3.3 Earthworm Optimization Algorithm (*EWA*)

The Earthworm Optimization Algorithm (EWA) is a metaheuristic optimization algorithm that mimics the burrowing behavior of earthworms in their search for food (Wang *et al*. 2018). The algorithm has been applied to a wide range of optimization problems. The EWA algorithm can be formulated as follows:

***Initialization*:** A set of *N* earthworms is randomly distributed in the search space. Each earthworm *i* is represented as a vector $x_i = [x_{1i}, x_{2i}, \ldots, x_{Di}]$, where *D* is the number of dimensions in the search space.

***Burrowing*:** Each earthworm moves in a random direction and distance based on the burrowing behavior of earthworms. The following equation determines the movement

$$x_i(t+1) = x_i(t) + r_i \times d \times \sin(\theta_i) \times \cos(\varphi_i) \tag{5}$$

where r_i is a random number between 0 and 1, d is the step size, θ_i and φ_i are random angles between 0 and 2π, and *t* is the current iteration number.

***Feeding*:** After burrowing, each earthworm evaluates the soil quality at its new location and updates its position accordingly. The quality of the soil is determined by the objective function being optimized. The fitness value of each earthworm is calculated using the following equation

$$f_i t_i = f(x_i) \tag{6}$$

where f(xi) is the objective function being optimized.

***Reproduction*:** The earthworms with higher fitness values are selected to reproduce and generate new earthworms. The reproduction process is based on the following equation

$$x_i(new) = x_i + \alpha \times (best_i - x_i) + \beta \times (worst_i - x_i) \tag{7}$$

where $x_i(new)$ is the new position of the earthworm *i*, $best_i$ is the position of the best earthworm in the

population, $worst_i$ is the position of the worst earthworm in the population, and α and β are two control parameters.

***Termination*:** The algorithm terminates when a stopping criterion is met, such as the maximum number of iterations or the target fitness value. The EWA algorithm has several advantages over other optimization algorithms. It is easy to implement, computationally efficient, and can handle many optimization problems. It has been applied to various issues, including function optimization, feature selection, and parameter tuning, and has shown promising results.

3.4 Future Search Algorithm (*FSA*)

Everyone in the world strives to live their best life. If someone feels that their life is not excellent, they will want to imitate the best person in the world. The upcoming search algorithm uses this characteristic to discover the best answers (Elsisi 2019). Equations used in mathematics are used to create the FSA. It uses the global search between the best people in history and the local search between people to update the random initial. The second HA begins its procedures randomly and constructs its iterations based on the best answer (Janamala *et al*. 2021). This causes the HA to undergo many iterations before finding the optimum answer, which may be far from the ideal option.

The FSA can solve this by adjusting every iteration and revealing random initials. A global best solution exists between each HA's multi-agent local and iterations. Some HA components update their new solutions in light of the most significant regional alternatives. The others, however, merely update their new solutions depending on the best global solution. These procedures could need several iterations. The FSA determines the optimal solutions by comparing local and worldwide best practices. A better solution may need more time and iterations to solve certain HA's more complex mathematical problems. The suggested FSA is created using straightforward mathematical formulas. People looking for the ideal living in many nations throughout the world are used in FSA to symbolize the space of solutions. The individual performing at the highest level in a nation represents the best local solution to the other individuals. This answer could vary yearly; a different individual may offer another one in a distinct nation. The person who performs the best over the years in a particular nation represents the best overall solution among the other people. The starting positions of each person will alter if their performance in a given year falls short of what it was the previous year.

The following mathematical equations serve as the foundation for this algorithm's technique. It bases its first stages on the equation's random answers

$$S(i,:) = Lb + (Ub - Lb) \cdot * rand(1,d) \tag{8}$$

If S is the solution, i is the population size solution, Lb and Ub are the upper and lower limits, *rand* is pseudo-random numbers spread uniformly, and d is the dimensions of the equation. The algorithm then starts doing its iterations to get the optimal answer. The best solution is picked, and after the solutions have been found, each one is defined as a local solution (*LS*), after which the best solution is characterized as a universal remedy (*GS*). The method specifies the answer for each population size component of the following equation, which depends on *GS* and *LS*.

First, the search in each nation is determined by the *LS* that supports the exploitation feature of the suggested method.

$$S(i,:)_L = \big(LS(i,:) - S(i,:)\big) * rand \tag{9}$$

Second, the proposed algorithm's *GS*, which facilitates exploration and is described as follows, determines how searches are conducted globally.

$$S(i,:)_G = \big(GS - S(i,:)\big) * rand \tag{10}$$

When the local and global convergences have been calculated, the result for each person is defined by

$$S(i,:) = S(i,:) + S(i,:)_L + S(i,:)_G \tag{11}$$

The algorithm then updates the GS and LS. The process adjusts the random initial of Eq. (1) after determining the solutions in the current iteration and the new *GS* and *LS*. This property characterizes the exploratory characteristic of the proposed method, which is enabled by

$$S(i,:) = GS + \big(GS - LS(i,:)\big) * rand \tag{12}$$

After initial updating, the algorithm assesses the *GS* and *LS*, and if they outperform the *GS* and *LS* of the main loop, they are updated.

4. Results and discussion

The present study examines the effectiveness of three innovative optimization techniques for determining the compressive strength of masonry constructions. This objective is achieved by integrating the algorithms with an MLP neural network. Each algorithm employs a specific search methodology to identify the ideal quantities for the computational weights associated with the MLP. The MLP is structured based on the size of its hidden layer and the number of neurons within it (Siow *et al*. 2023). Therefore, optimizing these parameters is crucial. Previous research has demonstrated that one hidden layer is sufficient for modeling complex phenomena (Feng *et al*. 2020). However, determining the optimal number of hidden neurons required a trial-and-error approach. The outcomes reveal that among the tested structures, where the middle layer ranges from 1 to 10 neurons, a structure with 6 × 5 × 1 neurons exhibited promising performance, as shown in Fig. 2.

4.1 Accuracy indicators

In the academic field of learning and prediction, the mean absolute error (MAE) and root mean square error (RMSE) are two of the most known metrics for measuring mistakes. Eqs. (9)-(10) are utilized to formulate these metrics. Eq. (11) also defines the coefficient of determination

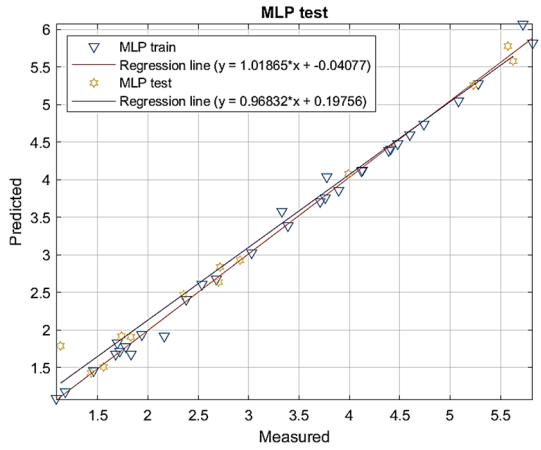

Fig. 4 Training and testing datasets accuracy results for various MLP structures

(R^2), which determines the compatibility between predicted and estimated masonry constructions' compressive strength.

$$MAE = \frac{1}{U}\sum_{i=1}^{U}\left|S_{i_{observed}} - S_{i_{predicted}}\right| \quad (13)$$

$$RMSE = \sqrt{\frac{1}{U}\sum_{i=1}^{U}\left[\left(S_{i_{observed}} - S_{i_{predicted}}\right)\right]^2} \quad (14)$$

$$R^2 = 1 - \frac{\sum_{i=1}^{U}\left(S_{i_{predicted}} - S_{i_{observed}}\right)^2}{\sum_{i=1}^{U}\left(S_{i_{observed}} - \underline{S}_{i_{observed}}\right)^2} \quad (15)$$

The equations presented involve two variables, $S_{i_{observed}}$ and $S_{i_{predicted}}$, which represent the measured and predicted total energy, respectively. Additionally, U denotes the quantity of data records utilized in the analysis. Moreover, $\underline{S}_{i_{observed}}$ refers to the mean value of the observed masonry constructions' compressive strength. As Fig. 4 shows, the amount of observed value in the training phase for RMSE is 0.10276, and for $R^{2,\,it}$ is 0.99735; in the testing phase, for RMSE, it is 0.10276 and for R^2 is 0.99331. So, we use MLP-ANN to improve these amounts.

4.2 Incorporated MLP with optimizers

Three ensembles are derived upon synthesizing the metaheuristic algorithms with the MLP: BHA-MLP, EWA-MLP, and FSA-MLP. These ensembles are trained with samples to establish a relationship between the compressive strength of masonry structures and the corresponding variables. To evaluate the optimization behavior of the methods, each model undergoes 1000 repetitions for implementation. The objective function is reported by calculating the RMSE of results at each repetition. It should be noted that this stage focuses on pattern recognition and reports RMSE of training data. The swarm-based algorithms rely significantly on the number of participants involved. The present study explores the performance of

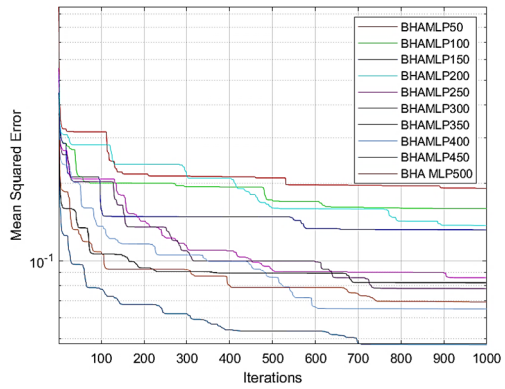

(a) BHAMLP

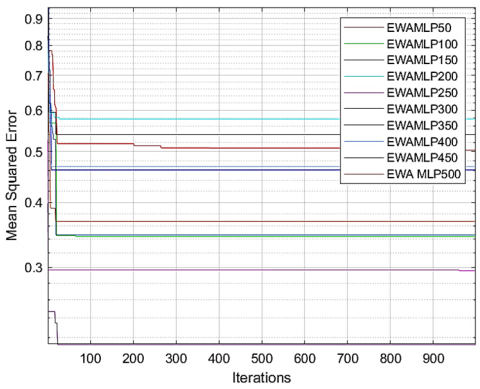

(b) EWAMLP

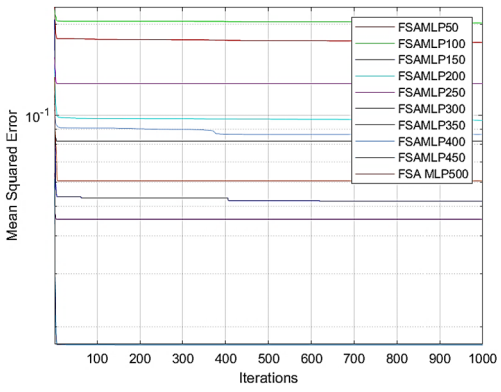

(c) FSAMLP

Fig. 5 The best-fit model for the (a) BHAMLP; (b) EWAMLP; and (c) FSAMLP

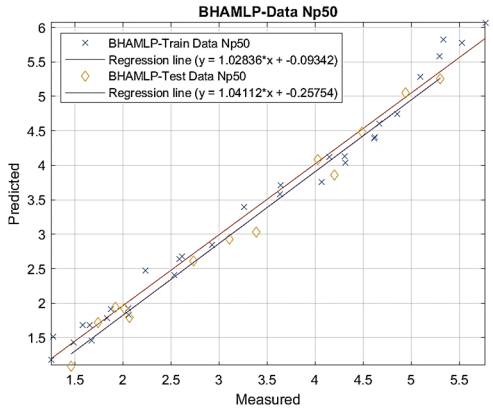

(a) BHAMLP- N_p50

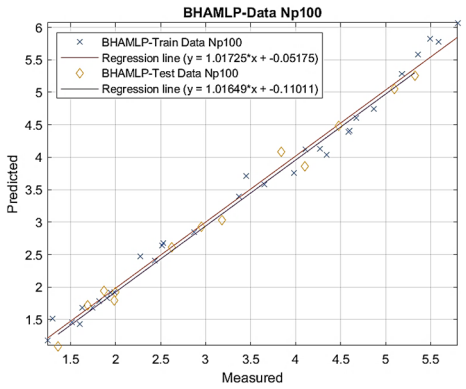

(b) BHAMLP - N_p100

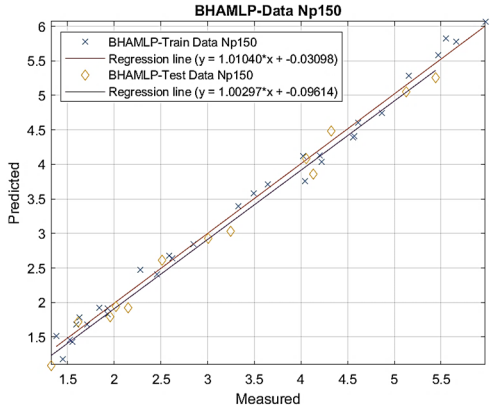

(c) BHAMLP - N_p150

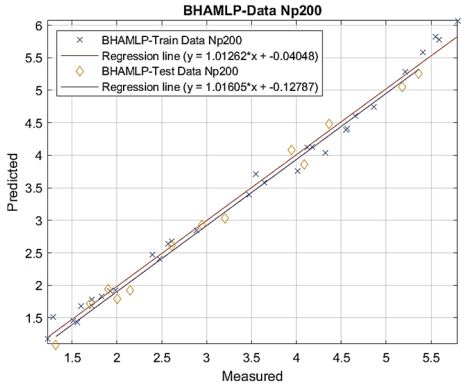

(d) BHAMLP - N_p 200

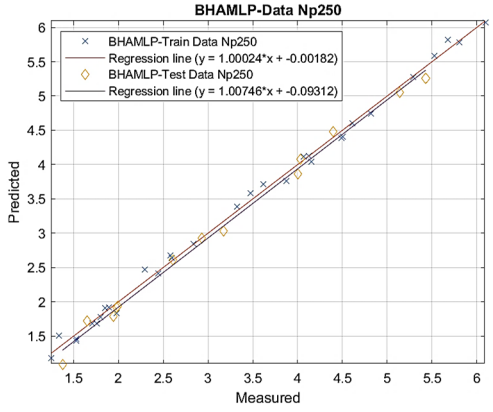

(e) BHAMLP - N_p250

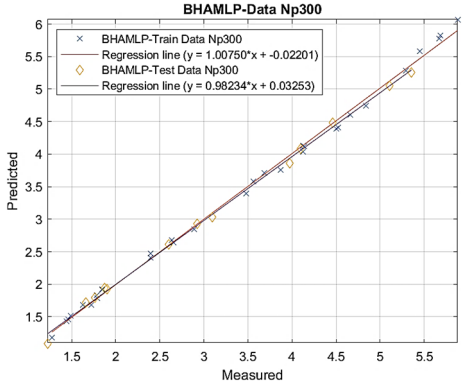

(f) BHAMLP - N_p300

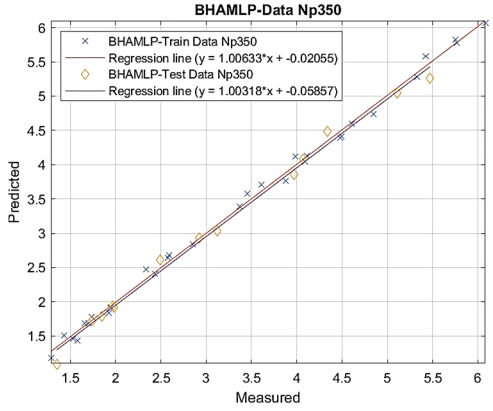

(g) BHAMLP - N_p350

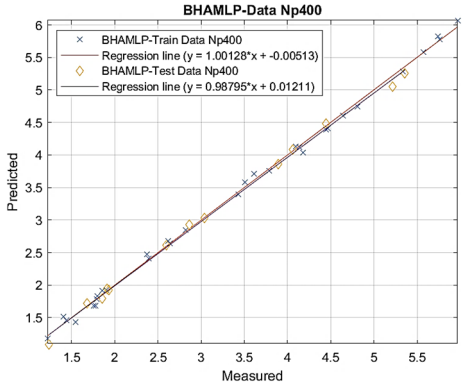

(h) BHAMLP - N_p400

Fig. 6 Training and testing datasets accuracy results for various BHAMLP-recommended structures

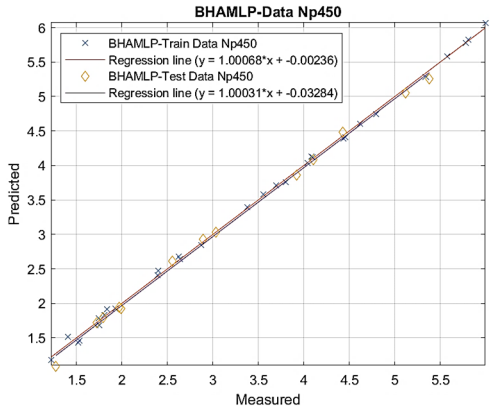

(i) BHAMLP - N_p450

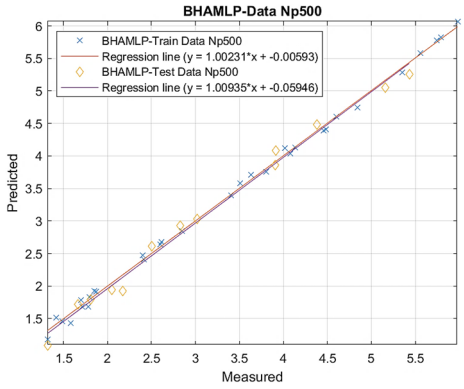

(j) BHAMLP - N_p500

Fig. 6 Continued

nine different population sizes (ranging from 50 to 500) for each model to identify the most optimal complexity that results in the lowest Mean Squared Error (MSE). The findings reveal that 450, 250, and 450 populations deliver the lowest RMSE and highest R^2 values for BHA-MLP, EWA-MLP, and FSA-MLP, respectively. These results are depicted in Fig. 5.

The generated models are accurate, simple to use, and agree significantly with the laboratory findings. This indicates how adaptable and reliable the created approach is. The best population size was determined by this research using a parametric analysis. Various MLP analyses were conducted on populations of 500, 450, 400, 350, 300, 250, 200, 150, 100, and 50 members.

A predictive neural network with a double hidden layer was trained with various node counts to identify the ideal MLP design. For each structure, the training procedure was repeated numerous times to demonstrate the replicability of the learning system. The three models shown in Tables 1 through 4 also underwent the same methodology. The

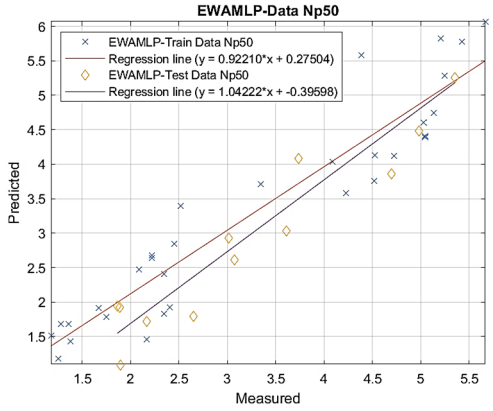

(a) EWAMLP- N_p50

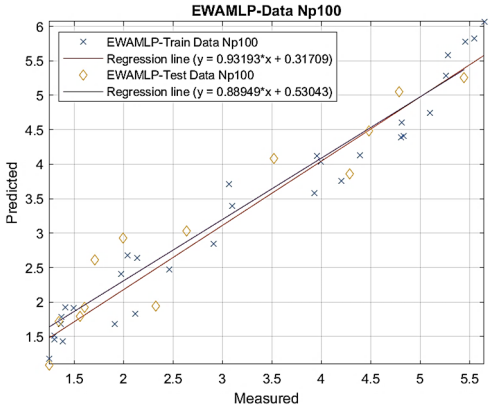

(b) EWAMLP - N_p100

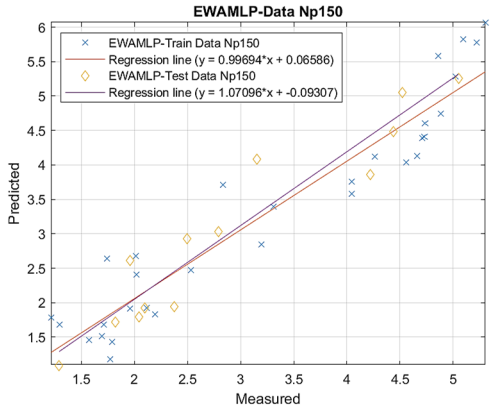

(c) EWAMLP - N_p150

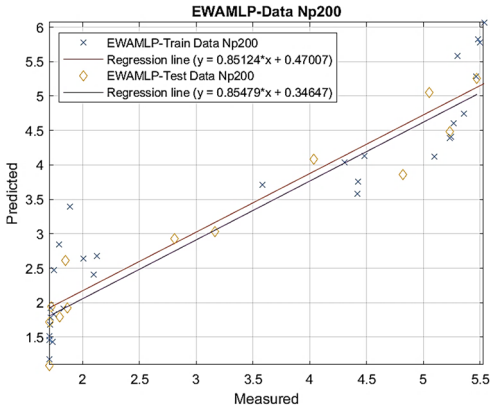

(d) EWAMLP - N_p 200

Fig. 7 Training and testing datasets accuracy results for various EWAMLP-recommended structures

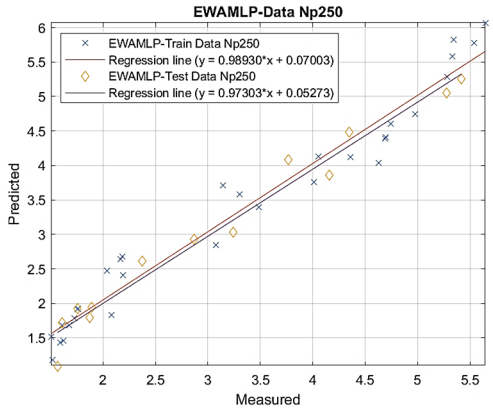

(e) EWAMLP - N_p250

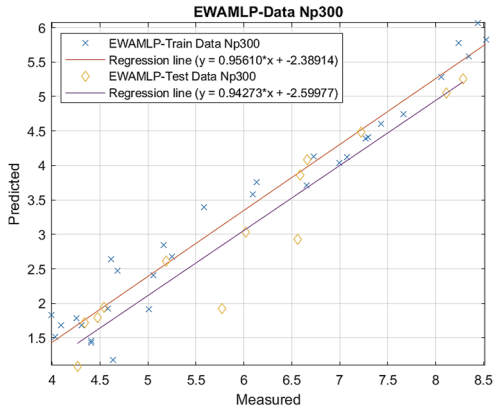

(f) EWAMLP - N_p300

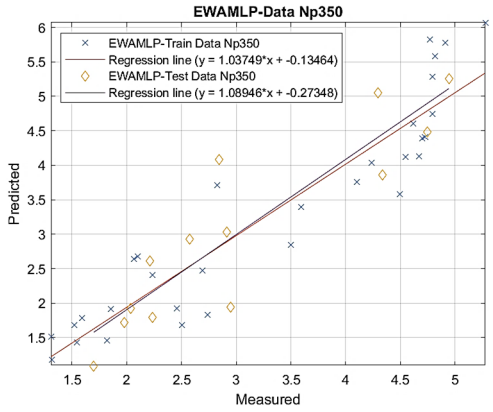

(g) EWAMLP - N_p350

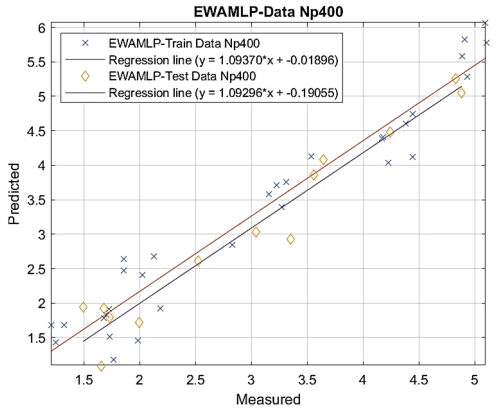

(h) EWAMLP - N_p400

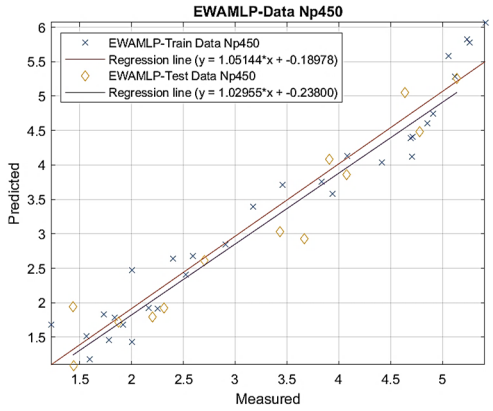

(i) EWAMLP - N_p450

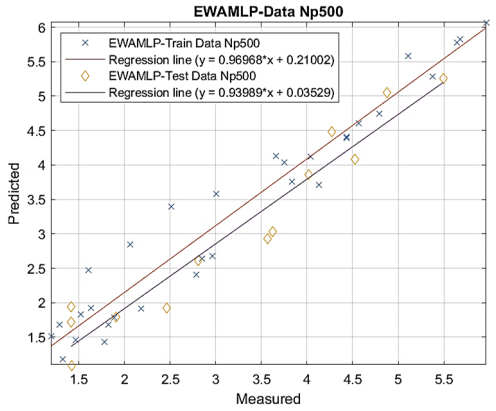

(j) EWAMLP - N_p500

Fig. 7 Continued

relationship between the quantity of neurons and the accuracy and complexity of network architectures is noteworthy. The results show that 450, 250, and 450 populations had the lowest RMSE values for BHA-MLP, EWA-MLP, and FSA-MLP. Based on the accuracy results of the testing outputs, a little increase in the value of testing R^2, and a slight decrease in the value of RMSE, the authors judged that a structure with four nodes was the best fit. As a result, the best structure for BHAMLP for all subsequent hybridization processes (including BHA-MLP, EWA-MLP, and FSA-MLP) was a 6*5*1 MLP architecture network organization.

4.3 Results

A scatter plot denotes a graphical representation that effectively showcases the correlation between two variables. Scatter plots are a tool for visualizing data in two dimensions, wherein each data point is depicted using a dot or symbol. One factor is plotted along the horizontal axis, while the other is plotted along the vertical axis. Such plots can be employed to discern patterns and trends within the data. These variables can demonstrate both the magnitude and orientation of their relationship. When the scatter plot's dots start to converge into a straight line, there is a significant connection between the two variables. If the dots

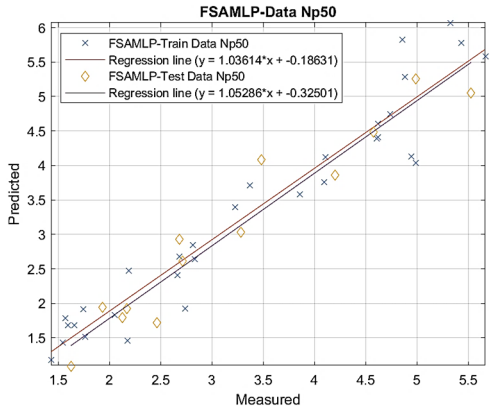

(a) FSAMLP- N_p50

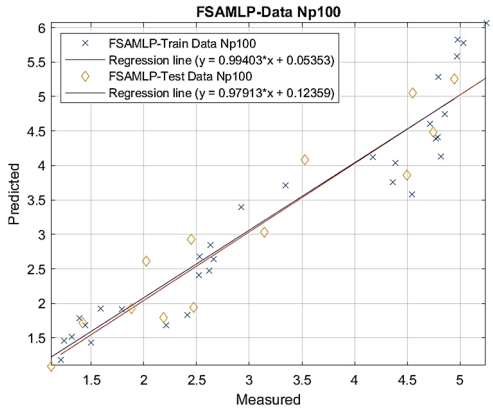

(b) FSAMLP - N_p100

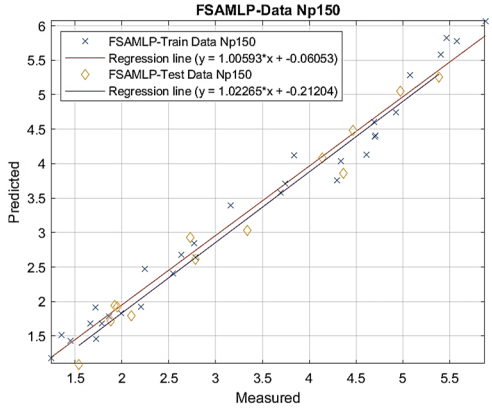

(c) FSAMLP - N_p150

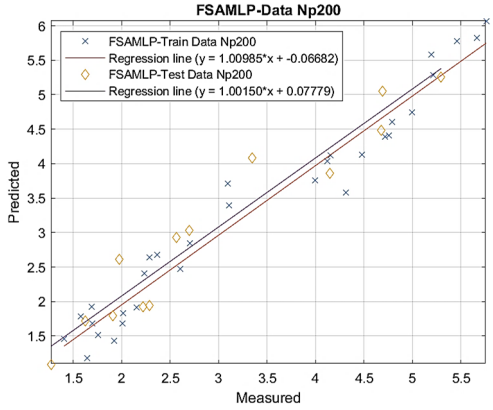

(d) FSAMLP - N_p 200

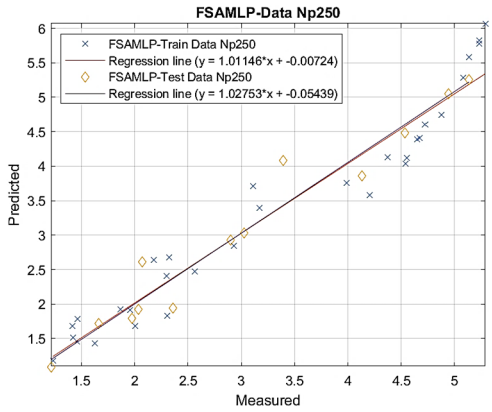

(e) FSAMLP - N_p250

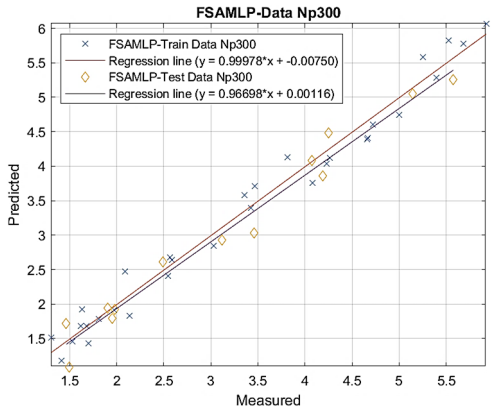

(f) FSAMLP - N_p300

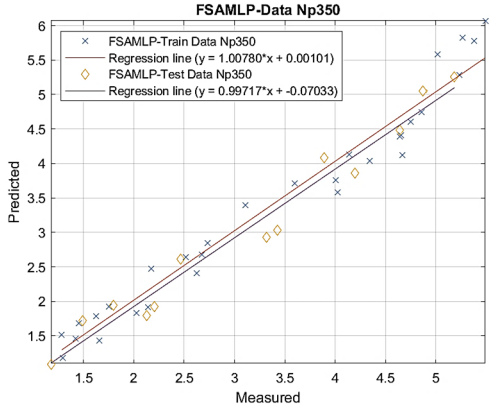

(g) FSAMLP - N_p350

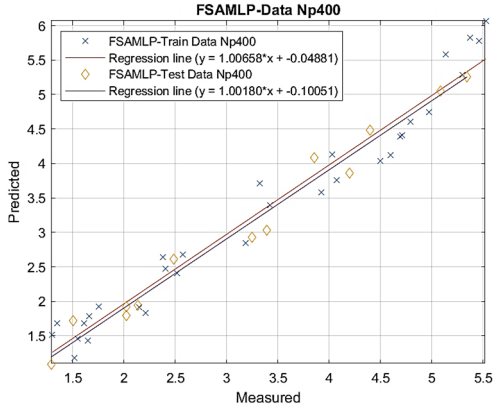

(h) FSAMLP- N_p400

Fig. 8 Training and testing datasets accuracy results for various FSAMLP-recommended structures

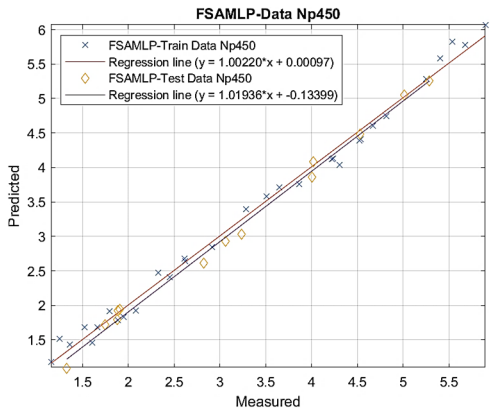

(i) FSAMLP - N_p450

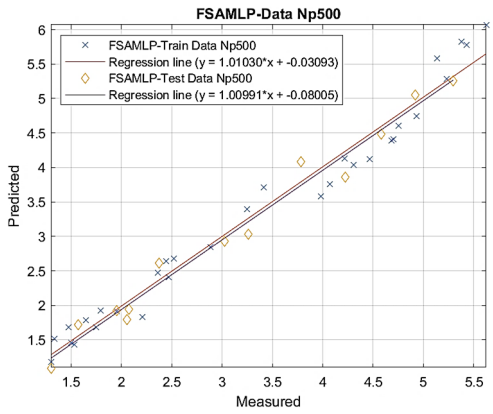

(j) FSAMLP - N_p500

Fig. 8 Continued

Table 2 Network findings for several planned BHAMLP swarm sizes based on two statistical metrics

Swarm size	Training dataset		Testing dataset		**Scoring**				Total score	Rank
	RMSE	R^2	RMSE	R^2	Training		Testing			
50	0.4868	0.9449	0.49358	0.92716	3	3	2	2	10	9
100	0.31178	0.9778	0.389	0.95541	8	8	4	4	24	6
150	0.45778	0.9514	0.39768	0.95335	4	4	3	3	14	8
200	0.52301	0.9361	0.37368	0.95893	2	2	6	6	16	7
250	0.29308	0.9804	0.21955	0.98601	10	10	10	10	40	1
300	0.30883	0.9782	0.38585	0.95614	9	9	5	5	28	3
350	0.53717	0.9324	0.57782	0.89867	1	1	1	1	4	10
400	0.36483	0.9694	0.29571	0.97448	5	5	9	9	28	3
450	0.33839	0.9737	0.34119	0.96588	7	7	8	8	30	2
500	0.34654	0.9724	0.34166	0.96578	6	6	7	7	26	5

Table 3 Network findings for several planned EWAMLP swarm sizes based on two statistical metrics

Swarm size	Training dataset		Testing dataset		**Scoring**				Total score	Rank
	RMSE	R^2	RMSE	R^2	Training		Testing			
50	0.40918	0.9614	0.34812	0.96445	2	2	3	3	10	9
100	0.44794	0.9535	0.41034	0.95025	1	1	1	1	4	10
150	0.22439	0.9885	0.19752	0.9887	8	8	7	7	30	3
200	0.30808	0.9783	0.35246	0.96354	4	4	2	2	12	8
250	0.35486	0.9711	0.28828	0.97576	3	3	4	4	14	7
300	0.21281	0.9897	0.21519	0.98657	9	9	6	6	30	3
350	0.28504	0.9814	0.23839	0.98349	6	6	5	5	22	6
400	0.2926	0.9804	0.19583	0.98889	5	5	8	8	26	5
450	0.1318	0.9961	0.09679	0.9973	10	10	10	10	40	1
500	0.24598	0.9862	0.19433	0.98906	7	7	9	9	32	2

are scattered randomly around the graph, this indicates a weak or no correlation. Scatter plots can also show any outliers or unusual values in the data. In the data analysis, an outlier refers to a specific data point that deviates considerably from the remaining dataset. These points can be crucial in identifying unusual trends or errors in the data.

Figs. 6-8 show the BHA-MLP, EWA-MLP, and FSA-MLP methods scatter plots. The calculated R^2s (0.9995, 0.9804, and 0.9961 in training and 0.99877, 0.98601 and 0.9973in the testing phase) and RMSE's (0.04731, 0.29308 and 0.1318 in training and 0.06537, 0.21955 and 0.09679 in testing phase) for population size 450, 250, and 450 give

Table 4 Network findings for several planned FSAMLP swarm sizes based on two statistical metrics

Swarm size	Training dataset		Testing dataset		**Scoring**				Total score	Rank
	RMSE	R^2	RMSE	R^2	Training		Testing			
50	0.40918	0.9614	0.34812	0.96445	2	2	3	3	10	9
100	0.44794	0.9535	0.41034	0.95025	1	1	1	1	4	10
150	0.22439	0.9885	0.19752	0.9887	8	8	7	7	30	3
200	0.30808	0.9783	0.35246	0.96354	4	4	2	2	12	8
250	0.35486	0.9711	0.28828	0.97576	3	3	4	4	14	7
300	0.21281	0.9897	0.21519	0.98657	9	9	6	6	30	3
350	0.28504	0.9814	0.23839	0.98349	6	6	5	5	22	6
400	0.2926	0.9804	0.19583	0.98889	5	5	8	8	26	5
450	0.1318	0.9961	0.09679	0.9973	10	10	10	10	40	1
500	0.24598	0.9862	0.19433	0.98906	7	7	9	9	32	2

Table 5 The performance of all four proposed methods using two statistical indices for network results

Method	Swarm size	Training dataset		Testing dataset		Scoring				Total score	Rank
		RMSE	R^2	RMSE	R^2	Training		Testing			
BHAMLP	450	0.04731	0.9995	0.06537	0.99877	3	3	3	3	12	1
EWAMLP	250	0.29308	0.9804	0.21955	0.98601	1	1	1	1	4	3
FSAMLP	450	0.1318	0.9961	0.09679	0.9973	2	2	2	2	8	2

a high accuracy in predicting the compressive strength of masonry structures.

Figs. 6-8 depict the regression line for the BHA-MLP, EWA-MLP, and FSA-MLP algorithms. It is comparable to the RMSE and R^2 values derived from Tables 1, 2, and 3 for population sizes 500, 450, 400, 350, 250, 300, 200, 150, 100, and 50. The iteration results revealed that BHA-MLP's prediction modeling was superior.

The accuracy of models in predicting the masonry constructions' compressive strength was evaluated based on their RMSE and R^2 values during both the learning and prediction phases. Tables 1-4 present all accuracy criteria obtained, with models exhibiting lower RMSE and higher R^2 selected as the most accurate predictors. The calculated RMSE (0.04731, 0.29308, and 0.1318 in training and 0.06537, 0.21955, and 0.09961 in the testing phase) give a high accuracy in predicting the compressive strength of masonry structures. Among these, the MLP constructed using weights and biases from BHA demonstrated the highest reliability and accuracy in predicting total energy without any discrepancy. Following this, FSA-MLP emerged as a promising optimizer for prediction, with EWA-MLP following behind.

- BHAMLP achieved the highest total score, indicating its superior performance among the three methods.
- It has the lowest RMSE and highest R^2 values for both training and testing datasets, which suggests that it provides the best fit to the data and the highest predictive accuracy.
- With a swarm size of 450, it used a relatively large number of iterations for optimization.
- EWAMLP achieved the lowest total score and is ranked third among the methods.
- It has the highest RMSE and relatively lower R^2 values than the other two methods for training and testing datasets, indicating a less accurate fit to the data.
- It used a swarm size of 250, smaller than BHAMLP and FSAMLP.
- FSAMLP falls between BHAMLP and EWAMLP in terms of performance, with a total score and rank of 8 and 2, respectively.
- It has moderately low RMSE and high R^2 values for training and testing datasets, suggesting good predictive capability.
- Similar to BHAMLP, it used a swarm size of 450.

BHAMLP performed the best in predictive accuracy, achieving the lowest RMSE and highest R^2 values for training and testing datasets. FSAMLP also performed well, securing the second rank. EWAMLP showed the lowest predictive accuracy and ranked third among the methods. The choice of which method to use depends on the application's specific requirements, available computational resources, and the desired level of accuracy.

As stated, this study segment evaluates the implemented models' efficacy by comparing their predicted masonry constructions' compressive strength output to the measured target values. The outcomes of the training and testing phases are depicted in Figs. 9-11, illustrating the variance of each piece of output and the intended use of the compressive strength of masonry structures and indicating

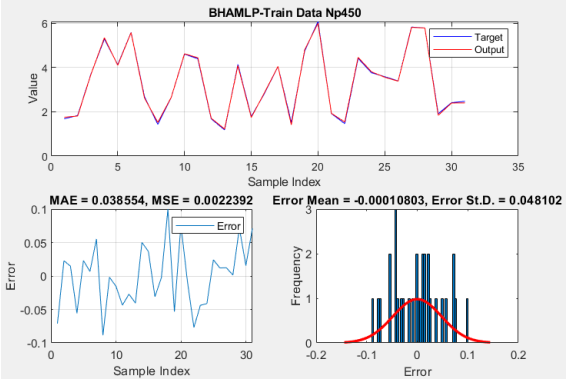

(a) BHAMLP 450-training

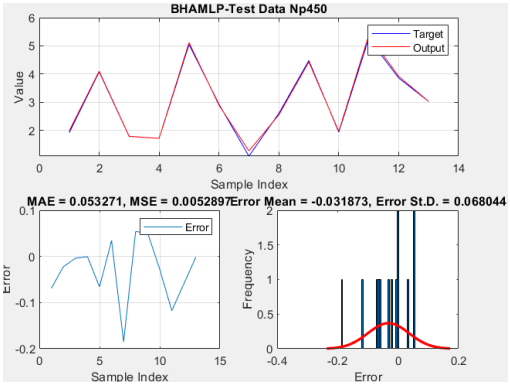

(b) BHAMLP 450-Testing

Fig. 9 The inaccuracy and frequency of MAE for the model best suited by BHAMLP

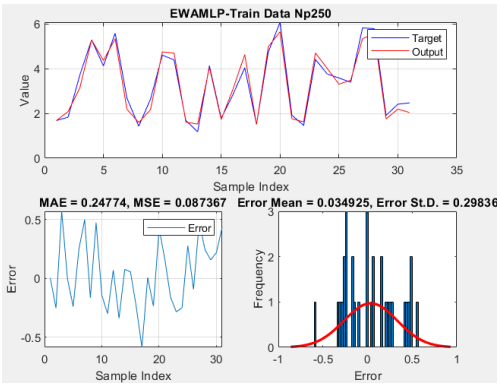

(a) EWAMLP 250-training

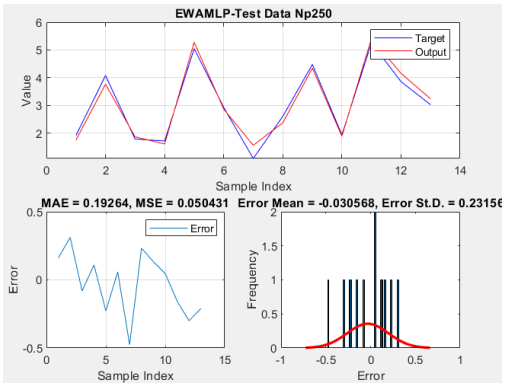

(b) EWAMLP 250-Testing

Fig. 10 The inaccuracy and frequency of MAE for the model best suited by EWAMLP

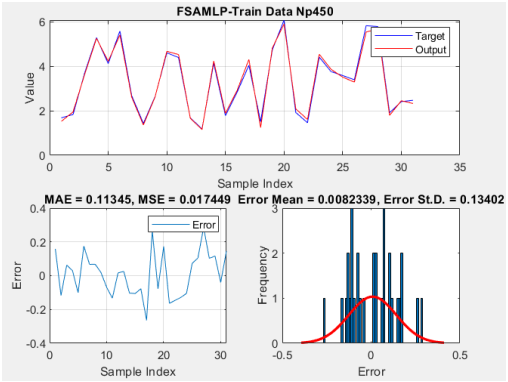

(a) FSAMLP 450-training

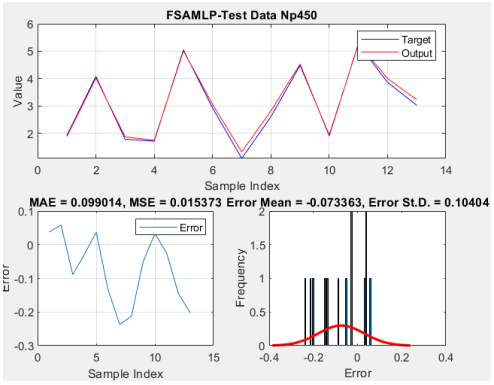

(b) FSAMLP 450-Testing

Fig. 11 The inaccuracy and frequency of MAE for the model best suited by FSAMLP

minimal training error for all three approaches. The R^2 values obtained demonstrate high consistency between the target and output total energy, with over 98% agreement observed. The testing outcomes are assessed based on the accuracy criteria cited. It is worth noting that the testing data are not initially provided to the networks. Thus, the findings in this section demonstrate the trained models' ability to assess the compressive strength of masonry structures under hypothetical scenarios. The testing outcomes are illustrated in Figs. 9(b)-11(b), accompanied by histogram charts that display the frequency of calculated error values.

The accuracy and reliability of the BHA-ANN method heavily depend on the quality and representativeness of the training data. Sufficient data collection from various masonry structures with diverse characteristics is crucial to ensure the model can generalize and provide accurate predictions. Additionally, proper preprocessing and normalization techniques should be applied to the data to enhance the training process. The architecture and

parameters of the MLP neural network play a significant role in the performance of the BHA-ANN method. The number of hidden layers, neurons in each layer, and the activation functions should be carefully chosen and optimized to achieve the best results.

Additionally, the training algorithm's learning rate, momentum, and stopping criteria should be appropriately tuned to avoid overfitting or underfitting. It is essential to validate the trained BHA-ANN model using independent test datasets to assess its performance accurately. Various evaluation metrics, such as mean squared error (MSE), root mean squared error (RMSE), and coefficient of determination (R-squared), can be used to measure the model's accuracy and compare it with other methods. Indeed, sensitivity analyses and cross-validation techniques can provide further insights into the model's robustness and generalizability. While the BHA-ANN method shows promise, it is essential to acknowledge certain limitations and challenges. The availability of high-quality training data, computational resources, and expertise in building and training ANN models may pose challenges in practical applications.

Additionally, the complexity of masonry structures, including variations in material properties, construction techniques, and environmental factors, can introduce uncertainties and affect the accuracy of predictions. Further research can explore enhancements to the BHA-ANN method, such as incorporating additional features or considering other factors affecting masonry structures' compressive strength. Comparative studies with different machine learning techniques or hybrid models can provide valuable insights into the performance and applicability of the BHA-ANN method. Additionally, investigating the potential of ANN in predicting other mechanical properties or failure modes of masonry structures can expand its utility in structural analysis and design.

ANN-based models can be a powerful tool to determine the compressive strength of masonry structures. However, choosing the correct method or algorithm is essential in this context. In determining the compressive strength of masonry structures, it is necessary to select the pressure measurement method according to the study's objectives and the type of masonry structure under investigation. An ANN-based model was a reliable, cheap, and straightforward approach to accurately modeling the compressive strength of masonry constructions. The present method has advantages in estimating the pressure of the structure. In terms of measurement, we can mention ease of use, speed of operation, and low cost of operation. In artificial intelligence-based models, such as neural networks, accurate and fast modeling is one of the beneficial features. This study presents a practical conventional technique for evaluating the compressive strength of masonry structures using the generated maps. In addition, the results showed that BHA-ANN gives more consistent results than the target. In conclusion, it is essential to mention that the high accuracy of the network outputs obtained from the experimental data set shows that all three developed networks are reliable enough and can be used to evaluate the masonry constructions' compressive strength in the future.

4.4 Taylor diagrams

A Taylor Diagram is a graphical tool used to evaluate the performance of different models or datasets by comparing them to a reference dataset. It is beneficial in fields like climate modeling, environmental science, and engineering, where multiple models or observations must be assessed for their accuracy in reproducing observed data. The Taylor Diagram is also an effective tool for visually summarizing the performance of models or datasets, helping researchers and engineers quickly assess accuracy and variability compared to a reference dataset.

A comparison framework in graphic form of several variables from one or more test data sets to one or more reference data sets is provided in Fig. 12 (the Taylor diagrams). While the test data sets are typically model experiments, the reference data set is frequently a control experiment or a collection of reference observations. The data depicted are often obtained from monthly, seasonal, or yearly climatological averages. The reference variables normalize the results since the various variables may have significantly varied numerical values. The normalized variance ratio reveals the relative amplitude of the predicted and actual deviations. Essential statistics for the conventional Taylor diagram are the weighted centered pattern correlation(s) and ratio(s) of the normalized root-

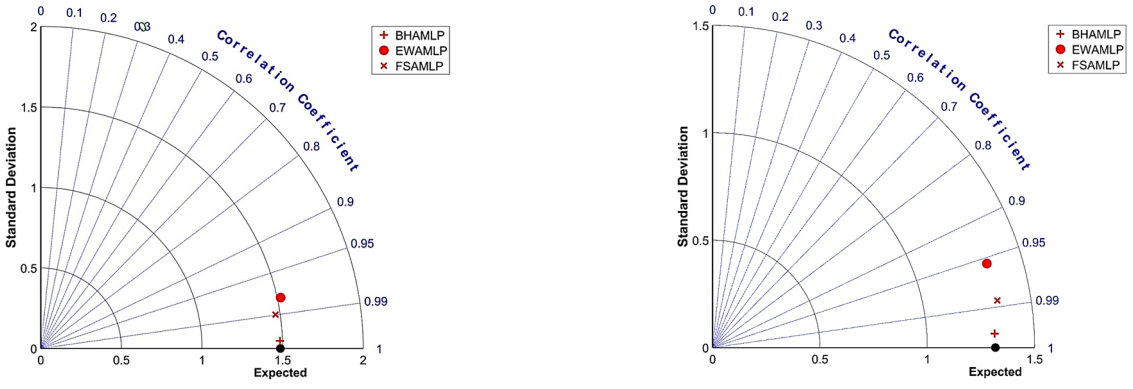

(a) Training datasets (b) Testing datasets

Fig. 12 Taylor diagrams (a) training datasets; (b) testing datasets

mean-square (RMS) discrepancies between "test" dataset(s) and "reference dataset(s)" (Taylor 2001).

5. Limitations and future work

While the results of this study demonstrate the potential of nature-inspired algorithms (BHA, EWA, and FSA) integrated with MLP models in predicting the compressive strength of masonry structures, certain limitations should be acknowledged. First, the dataset used in this study, although diverse, was limited in size and scope. This may affect the generalizability of the results to a broader range of masonry structures, materials, and environmental conditions. Expanding the dataset to include more varied structural types and geographical locations would enhance the robustness and applicability of the models. Second, the study primarily focused on static input parameters, such as dimensions and material properties, without accounting for dynamic factors like temperature variations, moisture content, or long-term degradation, which can significantly impact compressive strength. Future work should explore incorporating such dynamic variables to increase the predictive accuracy of the models.

Additionally, the models developed in this study were based on offline data processing, limiting their potential for real-time application. Future research should investigate the integration of these nature-inspired algorithms into real-time monitoring systems for innovative structures, allowing for continuous assessment and adjustment of structural parameters to ensure long-term performance and safety. Finally, while the models performed well based on RMSE and R^2 metrics, exploring additional performance indicators, such as computational efficiency and model stability under varying conditions, will provide a more comprehensive evaluation of the algorithms' practicality for large-scale implementation.

6. Conclusions

This study aimed to evaluate the predictive capabilities of three nature-inspired algorithms—BHA, EWA, and FSA—when combined with MLP models to estimate the compressive strength of masonry structures. The results demonstrate that the BHA-MLP model provided the most accurate predictions, achieving an R^2 of 0.9995 in the training phase and 0.99877 in the testing phase. FSA-MLP was the second-best model, showing strong performance across both datasets, while EWA-MLP, although slightly less accurate, still produced acceptable results.

This study underscores the effectiveness of these nature-inspired algorithms for improving compressive strength prediction, providing valuable insights for optimizing structural designs in masonry construction. The successful implementation of these models suggests that nature-inspired algorithms can be integral to developing more accurate, reliable structural predictions. Future research should focus on expanding the datasets to include a broader range of masonry structures and environmental variables. Additionally, incorporating these models into real-time decision-making systems for smart structures could enhance their practical applicability, leading to safer, more resilient construction practices in the industry.

References

Ahmadi Dehrashid, A., Dong, H., Fatahizadeh, M., Gholizadeh Touchaei, H., Gör, M., Moayedi, H., Salari, M. and Thi, Q.T. (2024), "A new procedure for optimizing neural network using stochastic algorithms in predicting and assessing landslide risk in East Azerbaijan", *Stochastic Environmental Research and Risk Assessment*, 1-30. https://doi.org/10.1007/s00477-024-02690-7

Algaifi, H.A., Bakar, S.A., Alyousef, R., Sam, A.R.M., Alqarni, A.S., Ibrahim, M., Shahidan, S., Ibrahim, M. and Salami, B.A. (2021), "Machine learning and RSM models for prediction of compressive strength of smart bio-concrete", *Smart Struct. Syst., Int. J.*, **28**(4), 535-551. https://doi.org/10.12989/sss.2021.28.4.535

Ali, A., Zhang, C., Bibi, T. and Sun, L. (2024), "Experimental investigation of sliding-based isolation system with re-centering functions for seismic protection of masonry structures", *Structures*, **60**, 105871. https://doi.org/10.1016/j.istruc.2024.105871

Alkayem, N.F., Shen, L., Mayya, A., Asteris, P.G., Fu, R., Di Luzio, G., Strauss, A. and Cao, M. (2023), "Prediction of concrete and FRC properties at high temperature using machine and deep learning: a review of recent advances and future perspectives", *J. Build. Eng.*, **83**, 108369. https://doi.org/10.1016/j.jobe.2023.108369

Alyami, M., Khan, M., Fawad, M., Nawaz, R., Hammad, A.W.A., Najeh, T. and Gamil, Y. (2024), "Predictive modeling for compressive strength of 3D printed fiber-reinforced concrete using machine learning algorithms", *Case Studies in Construction Materials*, **20**, e02728. https://doi.org/10.1016/j.cscm.2023.e02728

Armaghani, D.J., Mamou, A., Maraveas, C., Roussis, P.C., Siorikis, V.G., Skentou, A.D. and Asteris, P.G. (2021), "Predicting the unconfined compressive strength of granite using only two nondestructive test indexes", *Geomech. Eng., Int. J.*, **25**(4), 317-330. https://doi.org/10.12989/gae.2021.25.4.317

Asteris, P.G., Apostolopoulou, M., Armaghani, D., Cavaleri, L., Chountalas, A., Guney, D., Hajihassani, M., Hasanipanah, M., Khandelwal, M. and Karamani, C. (2020), "On the metaheuristic models for the prediction of cement-metakaolin mortars compressive strength", **11**(1), 063. https://doi.org/10.12989/mca.2020.1.1.063

Asteris, P.G., Koopialipoor, M., Armaghani, D.J., Kotsonis, E.A. and Lourenço, P.B. (2021), "Prediction of cement-based mortars compressive strength using machine learning techniques", Neural Computing and Applications, **33**(19), 13089-13121. https://doi.org/10.1007/s00521-021-06004-8

Asteris, P.G., Karoglou, M., Skentou, A.D., Vasconcelos, G., He, M., Bakolas, A., Zhou, J. and Armaghani, D.J. (2024), "Predicting uniaxial compressive strength of rocks using ANN models: Incorporating porosity, compressional wave velocity, and schmidt hammer data", *Ultrasonics*, **141**, 107347. https://doi.org/10.1016/j.ultras.2024.107347

Bilgehan, M. and Turgut, P. (2010), "The use of neural networks in concrete compressive strength estimation", *Comput. Concrete, Int. J.*, **7**(3), 271-283. https://doi.org/10.12989/cac.2010.7.3.271

Bogas, J.A., Gomes, M.G. and Gomes, A. (2013), "Compressive strength evaluation of structural lightweight concrete by

nondestructive ultrasonic pulse velocity method", *Ultrasonics*, **53**(5), 962-972. https://doi.org/10.1016/j.ultras.2012.12.012

Brencich, A. and Sterpi, E. (2006), "Compressive strength of solid clay brick masonry: calibration of experimental tests and theoretical issues", *Struct. Anal. Histor. Constr.*, 1-8.

Cao, J., Du, J., Zhang, H., He, H., Bao, C. and Liu, Y. (2024), "Mechanical properties of multi-bolted Glulam connection with slotted-in steel plates", *Constr. Build. Mater.*, **433**, 136608. https://doi.org/10.1016/j.conbuildmat.2024.136608

Chai, S., Wang, S., Liu, C., Liu, X., Liu, T. and Yang, R. (2024), "A visual measurement algorithm for vibration displacement of rotating body using semantic segmentation network", *Expert Syst. Applicat.*, **237**, 121306. https://doi.org/10.1016/j.eswa.2023.121306

Charter, I. (2003), "Principles for the analysis, conservation and structural restoration of architectural heritage", *Proceedings of the ICOMOS 14th General Assembly in Victoria Falls*, Victoria Falls, Zimbabwe, pp. 27-31.

Chen, R.-S., Zhang, H.-Y., Hao, X.-K., Yu, H.-X., Shi, T., Zhou, H.-S., Wang, R.-B., Zhao, Z.-F. and Wang, P. (2024), "Experimental study on ultimate bearing capacity of short thin-walled steel tubes reinforced with high-ductility concrete", *Structures*, **68**, 107109. https://doi.org/10.1016/j.istruc.2024.107109

Christopher, C.G., Pachaivannan, P. and Elamparithi, P.N. (2023), "Study on self-compacting polyester fiber reinforced concrete and strength prediction using ANN", *Adv. Concrete Constr., Int. J.*, **15**(2), 85. https://doi.org/10.12989/acc.2023.15.2.085

Elsisi, M. (2019), "Future search algorithm for optimization", Evolutionary Intelligence, **12**(1), 21-31. https://doi.org/10.21203/rs.3.rs-2769987/v1

Faghfouri, A., Vosoughifar, H. and Hosseininejad, S. (2023), "Optimal sensor placement of retrofitted concrete slabs with nanoparticle strips using novel DECOMAC approach", *Smart Struct. Syst., Int. J.*, **31**(6), 545-559. http://doi.org/10.12989/sss.2023.31.6.545

Feng, X., Ma, G., Su, S.-F., Huang, C., Boswell, M.K. and Xue, P. (2020), "A multilayer perceptron approach for accelerated wave forecasting in Lake Michigan", *Ocean Eng.*, **211**, 107526. https://doi.org/10.1016/j.oceaneng.2020.107526

Haddadvand, R., Sohrabi, N., Yan, T.X., Nadalinia, F. and Karouei, S.H.H. (2024), "Numerical study on the influence of flow direction and fluid type on heat transfer and pressure drop in a two-tube spiral heat exchanger with innovative conical turbulators", *Case Stud. Thermal Eng.*, **61**, 104933. https://doi.org/10.1016/j.csite.2024.104933

Hagan, M.T., Demuth, H.B. and Beale, M. (1997), Neural network design, PWS Publishing Co.

Hornik, K., Stinchcombe, M. and White, H. (1989), "Multilayer feedforward networks are universal approximators", *Neural networks*, **2**(5), 359-366. https://doi.org/10.1016/0893-6080(89)90020-8

Huang, H., Guo, M., Zhang, W., Zeng, J., Yang, K. and Bai, H. (2021), "Numerical investigation on the bearing capacity of RC columns strengthened by HPFL-BSP under combined loadings", *J. Build. Eng.*, **39**, 102266. https://doi.org/10.1016/j.jobe.2021.102266

Janamala, V., Kamal Kumar, U. and Pandraju, T.K.S. (2021), "Future search algorithm for optimal integration of distributed generation and electric vehicle fleets in radial distribution networks considering techno-environmental aspects", SN Applied Sciences, **3**(4), 464. https://doi.org/10.1007/s42452-021-04466-y

Kardani, N., Bardhan, A., Samui, P., Nazem, M., Asteris, P.G. and Zhou, A. (2022), "Predicting the thermal conductivity of soils using integrated approach of ANN and PSO with adaptive and time-varying acceleration coefficients", *Int. J. Thermal Sci.*, **173**, 107427. https://doi.org/10.1016/j.ijthermalsci.2021.107427

Köksal, H.O., Karakoç, C. and Yildirim, H. (2005), "Compression behavior and failure mechanisms of concrete masonry prisms", *J. Mater Civil Eng.*, **17**(1), 107-115. https://doi.org/10.1061/(ASCE)0899-1561(2005)17:1(107)

Koopialipoor, M., Asteris, P.G., Mohammed, A.S., Alexakis, D.E., Mamou, A. and Armaghani, D.J. (2022), "Introducing stacking machine learning approaches for the prediction of rock deformation", *Transport. Geotech.*, **34**, 100756. https://doi.org/10.1016/j.trgeo.2022.100756

Kubat, M. (1995), "Neural networks and fuzzy systems: A dynamical systems approach to machine intelligence", by Bart Kosko, Prentice Hall, Englewood Cliffs, NJ, USA, pp. 449,£ 24.96, ISBN 0-13-612334, The Knowledge Engineering Review **10**(2), 219-220. http://doi:10.1017/S0269888900008225

Kumar, S., Datta, D. and Singh, S.K. (2015), "Black hole algorithm and its applications", *Computat. Intell. Applicat. Model. Control*, 147-170. http://doi.org/10.1007/978-3-319-11017-2_7

Liou, S.-W., Wang, C.-M. and Huang, Y.-F. (2009), "Integrative Discovery of Multifaceted Sequence Patterns by Frame-Relayed Search and Hybrid PSO-ANN", *J. Univers. Comput. Sci.*, **15**(4), 742-764.

Lu, D., Wang, G., Du, X. and Wang, Y. (2017), "A nonlinear dynamic uniaxial strength criterion that considers the ultimate dynamic strength of concrete", *Int. J. Impact Eng.*, **103**, 124-137. https://doi.org/10.1016/j.ijimpeng.2017.01.011

Marani, A. and Nehdi, M.L. (2020), "Machine learning prediction of compressive strength for phase change materials integrated cementitious composites", *Constr. Build. Mater.*, **265**, 120286. https://doi.org/10.1016/j.conbuildmat.2020.120286

Masi, A. and Chiauzzi, L. (2013), "An experimental study on the within-member variability of in situ concrete strength in RC building structures", *Constr. Build. Mater.*, **47**, 951-961. https://doi.org/10.1016/j.conbuildmat.2013.05.102

McCord-Nelson, M. and Illingworth, W.T. (1991), *A practical guide to neural nets*, Addison-Wesley Longman Publishing Co., Inc.

Mishra, M., Bhatia, A.S. and Maity, D. (2020a), "Predicting the compressive strength of unreinforced brick masonry using machine learning techniques validated on a case study of a museum through nondestructive testing", *J. Civil Struct. Health Monitor.*, **10**(3), 389-403. https://doi.org/10.1007/s13349-020-00391-7

Mishra, P., Samui, P. and Sinha, S. (2020b), "Determination of reliability index of the retaining wall using artificial intelligence techniques", *Metaheur. Comput. Applicat., Int. J.*, **1**(1), 043. https://doi.org/10.12989/mca.2020.1.1.043

Mishra, M., Bhatia, A.S. and Maity, D. (2021), "A comparative study of regression, neural network and neuro-fuzzy inference system for determining the compressive strength of brick–mortar masonry by fusing nondestructive testing data", *Eng. Comput.*, **37**(1), 77-91. https://doi.org/10.1007/s00366-019-00810-4

Moayedi, H. and Khasmakhi, M.A.S.A. (2022), "Wildfire susceptibility mapping using two empowered machine learning algorithms", *Stochast. Environ. Res. Risk Assess.*, **37**, 49-72. https://doi.org/10.1007/s00477-022-02273-4

Moayedi, H. and Le, B.N. (2024), "The development of four efficient optimal neural network methods in forecasting shallow foundation", *Comput. Concrete, Int. J.*, **34**(2), 151-168. https://doi.org/10.12989/cac.2024.34.2.151

Moayedi, H., Ghareh, S. and Foong, L.K. (2022), "Quick integrative optimizers for minimizing the error of neural computing in pan evaporation modeling", *Eng. Comput.*, **38**(2), 1331-1347. https://doi.org/10.1007/s00366-020-01277-4

Moayedi, H., Ahmadi Dehrashid, A. and Nguyen Le, B. (2024), "A

novel problem-solving method by multi-computational optimisation of artificial neural network for modelling and prediction of the flow erosion processes", *Eng. Applicat. Computat. Fluid Mech.*, **18**(1), 2300456. https://doi.org/10.1080/19942060.2023.2300456

Poorisat, T., Aigwi, I.E., Doan, D.T. and GhaffarianHoseini, A. (2024), "Unlocking the potentials of sustainable building designs and practices: A Systematic Review", *Building and Environment*, **266**, 112069. https://doi.org/10.1016/j.buildenv.2024.112069

Ronghui, S. and Liangrong, N. (2022), "An intelligent fuzzy-based hybrid metaheuristic algorithm for analysis the strength, energy and cost optimization of building material in construction management", *Eng. Comput.*, **38**(4), 2663-2680. https://doi.org/10.1007/s00366-021-01420-9

Sabbağ, N. and Uyanık, O. (2017), "Prediction of reinforced concrete strength by ultrasonic velocities", *J. Appl. Geophys.*, **141**, 13-23. https://doi.org/10.1016/j.jappgeo.2017.04.005

Shu, J., Yu, H., Liu, G., Duan, Y., Hu, H. and Zhang, H. (2025), "DF-CDM: Conditional diffusion model with data fusion for structural dynamic response reconstruction", *Mech. Syst. Signal Process.*, **222**, 111783. https://doi.org/10.1016/j.ymssp.2024.111783

Siow, P.Y., Ong, Z.C., Khoo, S.Y., Lim, K.-S. and Chew, B.T. (2023), "Hybrid machine learning with mode shape assessment for damage identification of plates", *Smart Struct. Syst., Int. J.*, **31**(5), 485-500. https://doi.org/10.12989/sss.2023.31.5.485

Sohrabi, N., Haddadvand, R. and Nabi, H. (2024), "Numerical investigation of the effect of fluid nanohybrid type and volume concentration of fluid on heat transfer and pressure drop in spiral double tube heat exchanger equipped with innovative conical turbulator", *Case Stud. Thermal Eng.*, **60**, 104751. https://doi.org/10.1016/j.csite.2024.104751

Sun, R., Wang, S., Li, M. and Zhu, Y. (2025), "An algorithm for large-span flexible bridge pose estimation and multi-keypoint vibration displacement measurement", *Measurement*, **240**, 115582. https://doi.org/10.1016/j.measurement.2024.115582

Taylor, K.E. (2001), "Summarizing multiple aspects of model performance in a single diagram", *J. Geophys. Res.: Atmospheres*, **106**(D7), 7183-7192. https://doi.org/10.1029/2000JD900719

Wang, Y. and Sigmund, O. (2023), "Multi-material topology optimization for maximizing structural stability under thermo-mechanical loading", *Comput. Methods Appl. Mech. Eng.*, **407**, 115938. https://doi.org/10.1016/j.jrmge.2023.11.025

Wang, Y. and Sigmund, O. (2024), "Topology optimization of multi-material active structures to reduce energy consumption and carbon footprint", *Struct. Multidiscipl. Optimiz.*, **67**(1), 5. https://doi.org/10.1007/s00158-023-03698-3

Wang, G.-G., Deb, S. and Coelho, L.D.S. (2018), "Earthworm optimisation algorithm: a bio-inspired metaheuristic algorithm for global optimisation problems", *Int. J. Bio-Inspired Computat.*, **12**(1), 1-22. https://doi.org/10.1504/IJBIC.2018.093328

Wang, G., Mukhtar, A., Moayedi, H., Khalilpoor, N. and Tt, Q. (2024), "Application and evaluation of the evolutionary algorithms combined with conventional neural network to determine the building energy consumption of the residential sector", *Energy*, **298**, 131312. https://doi.org/10.1016/j.energy.2024.131312

Wu, Z., Moayedi, H., Salari, M., Le, B.N. and Ahmadi Dehrashid, A. (2024), "Assessment of sodium adsorption ratio (SAR) in groundwater: Integrating experimental data with cutting-edge swarm intelligence approaches", *Stochast. Environ. Res. Risk Assess.*, 1-18. https://doi.org/10.1007/s00477-024-02727-x

Ye, D., Ahmadi Dehrashid, H., Moayedi, H. and Ahmadi Dehrashid, A. (2024), "Investigating the spatial foundations of rural entrepreneurship development using a hybrid method of MCDM, ANN and DTree algorithm", *Environ. Develop. Sustainabil.*, 1-33. https://doi.org/10.1007/s10668-024-04739-7

Yoon, S. and Lee, Y.-J. (2023), "A surrogate model-based framework for seismic resilience estimation of bridge transportation networks", *Smart Struct. Syst., Int. J.*, **32**(1), 49-59. https://doi.org/10.12989/sss.2023.32.1.049

Zhao, Y., Moayedi, H., Foong, L.K. and Thi, Q.T. (2024), "Slime mold and four other nature-inspired optimization algorithms in analyzing the concrete compressive strength", *Smart Struct. Syst., Int. J.*, **33**(1), 65-91. https://doi.org/10.12989/sss.2024.33.1.065

Zhou, X., Lu, D., Du, X., Wang, G. and Meng, F. (2020), "A 3D non-orthogonal plastic damage model for concrete", *Comput. Methods Appl. Mech. Eng.*, **360**, 112716. https://doi.org/10.1016/j.cma.2019.112716

Zurada, J. (1992), *Introduction to artificial neural systems*, West Publishing Co.

Abbreviation

Phrase	Abbreviation
Multilayer Perceptron	MLP
Artificial Neural Network	ANN
Black hole algorithm (BHA)	BHA
Earthworm optimization algorithm (EWA)	EWA
Future search algorithm (FSA)	FSA
Whale Optimization Algorithm	WOA
Root Mean Square Error	RMSE
International Council of Monuments and Sites	ICOMOS
Ground Penetrating Radar	GPR
Nondestructive testing	NDT
Rebound Hammer	RH
Ultrasonic Pulse Velocity	UPV